Assessment of gravity wave momentum flux measurement capabilities by meteor radars having different transmitter power and antenna configurations

D. C. Fritts,[1,2] D. Janches,[3] W. K. Hocking,[4] N. J. Mitchell,[5] and M. J. Taylor[6]

Received 16 November 2011; revised 25 March 2012; accepted 28 March 2012; published 19 May 2012.

[1] Measurement capabilities of five meteor radars are assessed and compared to determine how well radars having different transmitted power and antenna configurations perform in defining mean winds, tidal amplitudes, and gravity wave (GW) momentum fluxes. The five radars include two new-generation meteor radars on Tierra del Fuego, Argentina (53.8°S) and on King George Island in the Antarctic (62.1°S) and conventional meteor radars at Socorro, New Mexico (34.1°N, 106.9°W), Bear Lake Observatory, Utah (~41.9°N, 111.4°W), and Yellowknife, Canada (62.5°N, 114.3°W). Our assessment employs observed meteor distributions for June of 2009, 2010, or 2011 for each radar and a set of seven test motion fields including various superpositions of mean winds, constant diurnal tides, constant and variable semidiurnal tides, and superposed GWs having various amplitudes, scales, periods, directions of propagation, momentum fluxes, and intermittencies. Radars having higher power and/or antenna patterns yielding higher meteor counts at small zenith angles perform well in defining monthly and daily mean winds, tidal amplitudes, and GW momentum fluxes, though with expected larger uncertainties in the daily estimates. Conventional radars having lower power and a single transmitting antenna are able to describe monthly mean winds and tidal amplitudes reasonably well, especially at altitudes having the highest meteor counts. They also provide reasonable estimates of GW momentum fluxes at the altitudes having the highest meteor counts; however, these estimates are subject to uncertainties of ~20 to 50% and uncertainties rapidly become excessive at higher and lower altitudes. Estimates of all quantities degrade somewhat for more complex motion fields.

Citation: Fritts, D. C., D. Janches, W. K. Hocking, N. J. Mitchell, and M. J. Taylor (2012), Assessment of gravity wave momentum flux measurement capabilities by meteor radars having different transmitter power and antenna configurations, *J. Geophys. Res.*, *117*, D10108, doi:10.1029/2011JD017174.

1. Introduction

[2] Gravity waves (GWs) play significant roles in atmospheric dynamics, chemistry, microphysics, and plasma processes extending from Earth's surface into the thermosphere and ionosphere. At lower altitudes, GWs contribute to boundary layer and mesoscale structures, organize convection, and induce turbulence and mixing of relevance to weather prediction and aircraft at flight altitudes. In the middle stratosphere, GWs induce polar stratospheric clouds that contribute to ozone destruction. Throughout the atmosphere, but especially at higher altitudes, GWs systematically influence the large-scale circulation and thermal structure via energy and momentum transport and deposition. These influences are typically slow and systematic at lower altitudes, but may be local and strong accompanying severe events. In the mesosphere and lower thermosphere (MLT), GWs lead to closure of the mesospheric jets, large departures from radiative equilibrium, strong turbulence and mixing of heat, momentum, and constituents, and significant interactions with, and influences on, tides and planetary waves. GWs are expected to have similar, but still largely unknown, effects higher in the thermosphere and ionosphere. Indeed, the vertical transport of horizontal momentum by GWs, and its deposition accompanying GW dissipation, account for the major influences of these motions on the mean and large-scale atmospheric circulation, structure, and variability. Reviews of these various dynamics emphasizing the higher

[1]Colorado Research Associates Division, NorthWest Research Associates, Boulder, Colorado, USA.
[2]Now at GATS/Boulder, Boulder, Colorado, USA.
[3]Space Weather Laboratory, NASA Goddard Space Flight Center, Greenbelt, Maryland, USA.
[4]Department of Physics, University of Western Ontario, London, Ontario, Canada.
[5]Centre for Space, Atmospheric and Oceanic Science, Department of Electronic and Electrical Engineering, University of Bath, Bath, UK.
[6]Department of Physics, Utah State University, Logan, Utah, USA.

Corresponding author: D. C. Fritts, GATS/Boulder, 3360 Mitchell Ln., Boulder, CO 80301, USA. (dave@gats-inc.com)

0148-0227/12/2011JD017174

altitudes are provided by *Hines* [1960], *Lighthill* [1978], *McIntyre* [1989], *Hocke and Schlegel* [1996], *Nappo* [2002], *Fritts and Alexander* [2003], *Kim et al.* [2003], *Fritts et al.* [2006a], and *Fritts and Lund* [2011].

[3] The various responses to momentum transport by GWs noted above make this a key quantity in understanding and modeling atmospheric structure at all altitudes. Consequently, significant efforts have addressed these dynamics employing theoretical, modeling, and observational methods, typically focusing on the higher altitudes where the effects of these dynamics are most pronounced [*Fritts and Alexander*, 2003]. Further quantification of these dynamics throughout the atmosphere also remains a major research need, given the importance of their proper parameterization for weather and climate forecasting [*Kim et al.*, 2003].

[4] Prior to new meteor radar capabilities, direct measurements of GW momentum fluxes have only been possible with Doppler radars or lidars having symmetric, relatively narrow, off-zenith coplanar beam pairs [*Vincent and Reid*, 1983; *Reid and Vincent*, 1987; *Fritts and Vincent*, 1987; *Fukao et al.*, 1988; *Reid et al.*, 1988; *Fritts and Yuan*, 1989; *Fritts et al.*, 1990, 1992, 2006b; *Fritts and Janches*, 2008; *Sato*, 1990, 1993, 1994; *Tsuda et al.*, 1990; *Wang and Fritts*, 1990, 1991; *Hitchman et al.*, 1992; *Nakamura et al.*, 1993; *Murayama et al.*, 1994; *Murphy and Vincent*, 1993, 1998; *Acott*, 2009] or via in situ measurements by aircraft at lower altitudes or chaff measurements in the MLT [e.g., *Lilly and Kennedy*, 1973; *Lilly et al.*, 1982; *Brown*, 1983; *Meyer et al.*, 1989; *Nastrom and Fritts*, 1992; *Smith et al.*, 2008]. Indirect methods have nevertheless contributed to quantification of, or constraints on, momentum fluxes employing airglow [e.g., *Swenson et al.*, 1999; *Fritts et al.*, 2002; *Espy et al.*, 2004, 2006], balloon [e.g., *Hertzog and Vial*, 2001; *Hertzog et al.*, 2008], and satellite measurements [e.g., *Ern et al.*, 2004]. These various measurements have revealed a variety of responses, including systematic seasonal-mean momentum fluxes accounting for large-scale forcing at lower and higher altitudes, responses to specific sources and source regions, episodic and strong forcing accompanying GWs that are transient and localized, but achieve large amplitudes, and significant filtering and interactions with larger-scale mean, tidal, and planetary wave (PW) motions.

[5] Ideally, routine momentum flux measurements would provide continuous sensitivity to the magnitudes that are dynamically important and also capture the temporal variations accompanying strong, but transient, events that may nevertheless contribute significantly to hourly, daily, monthly, and seasonal means. Improved understanding and parameterization of GW influences also impose a need for such measurements at a range of locations spanning representative source regions for GWs and the environments in which they propagate. Unfortunately, those systems that do (or did) have such measurement capabilities are very limited, their costs are very high (typically ~$1 M to 10 M, with several much more costly), and very few measure continuously. Furthermore, only two sodium resonance lidars (to our knowledge), one at the Arctic Lidar Observatory for Middle Atmosphere Research (ALOMAR) at 69.3°N in Norway and the other at the Andes Lidar Observatory (ALO) at 30°S in Chile, are even at the edges of regions of identified high seasonal GW activity extending into the stratosphere and MLT. So there are considerable motivations for exploring other measurement techniques that may offer the potential to significantly expand such measurements with much cheaper systems. Such systems should also have the potential for continuous measurements; optical systems, whether active (lidar) or passive (airglow, FPI, etc.) cannot provide full diurnal and annual measurements, independent of weather, suggesting that only radar measurements are likely to address this need.

[6] The Southern Argentina Agile MEteor Radar (SAAMER) [*Fritts et al.*, 2010a] (hereafter *F10a*) was specifically designed to add a potential for GW momentum flux measurements to the conventional meteor radar capabilities for mean, tidal, and PW measurements for the reasons noted above. This was accomplished by devising a radar beam pattern that yielded a majority of meteors at zenith angles <50° and employing high power to achieve as high a meteor rate as possible at these angles. SAAMER was installed at Rio Grande on Tierra del Fuego, Argentina (53.8°S, 67.7°W) and became operational in May 2008. SAAMER momentum flux measurement capabilities were evaluated using observed meteor distributions for September 2008. This utilized a series of test motion fields including prescribed mean winds, diurnal and semidiurnal tide winds, and GWs having various spatial and temporal scales [*Fritts et al.*, 2010b] (hereafter *F10b*), and the analysis procedure suggested by *Hocking* [2005] employing a "full-field" fit to the various winds, variances, and covariances characterizing the superposed mean winds, tides, and GWs. These tests suggested that for real wind fields having similar composition and character to the test fields, SAAMER should be expected to provide very good definition of the mean and tidal winds and reasonably good definition of GW momentum fluxes where meteor count rates are sufficient.

[7] The apparent success of SAAMER (on Tierra del Fuego, Argentina, hereafter TdF) in measuring GW momentum fluxes in addition to mean, tidal, and PW winds was the motivation for a SAAMER clone, the Drake Antarctic Agile MEteor Radar (DrAAMER) that was installed at the Brazilian Antarctic Comandante Ferraz Base (62.1°S, 58.7°W) on King George Island (hereafter KGI) in March 2010. Comparisons of the mean and tidal winds and the GW momentum fluxes measured by SAAMER and DrAAMER by *Fritts et al.* [2012] demonstrated close correspondence between mean and tidal winds at the two sites, as well as significant similarities between the inferred GW momentum fluxes between years and sites from April to June of 2010 and 2011. This agreement suggested significant confidence in the GW momentum flux measurement potential for both radars, given the tests performed with SAAMER data. Nevertheless, we believe it is important to subject DrAAMER to the same tests applied to SAAMER. We also believe that applications of these tests to additional meteor radars having different characteristics (particularly power and beam configuration) may help us identify what radar capabilities are required to achieve GW momentum flux measurements that are sufficiently accurate to be valuable to the community. For example, the *Hocking* [2005] analysis method was tested with meteor radar data from Socorro, NM and Resolute Bay, Canada and judged to provide reasonable two-month estimates (though without validation). Other meteor radars have also been employed for GW variance, momentum flux, and tidal modulation studies and suggest that more radars may provide

Table 1. Radar Characteristics for the Five Radars Employed in This Evaluation of Measurement Capabilities[a]

Radar	Location (lat/long)	Frequency, Bandwidth	Peak Power	Resolution	TX/RX Antennas	PRF (Hz)	Coding, Integration	Meteors/Day
DrAAMER (KGI)	(62.1°S, 58.7°W)	36.9 MHz, 35–125 kHz	30 kW	2 km	8/5, 3-ele. cross. Yagis	1730	2 bit, 4 samp.	~9,000
SAAMER (TdF)	(53.8°S, 67.7°W)	32.55 MHz, 50–250 kHz	60 kW	2 km	8/8, 3-ele. cross. Yagis	2144, 1730	2 bit, 4 samp.	~14,000
Socorro, NM (SOC)	(34.1°N, 106.9°W)	35.24 MHz, 35–125 kHz	6 kW	2 km	1/5, 2-ele. Yagis	2140	1 bit, 8 samp.	~5,000
Bear Lake, UT (BLO)	(41.9°N, 111.4°W)	35.24 MHz, 50–250 kHz	12 kW	2 km	1/5, 2-ele. cross. Yagis	2140	1 bit, 4 samp.	~11,000
Yellowknife, Canada (YK)	(62.5°N, 114.3°W)	35.65 MHz, 50–125 kHz	6 kW	2 km	1/5, 2-ele. Yagis	2140	1 bit, 8 samp.	~2,500

[a]Meteor counts for zenith angles between 15 and 50° are ~50% of the total counts (Meteors/Day column) for KGI and TdF and ~30% of the total counts for the other radars.

enhanced measurement capabilities with testing and suitable analysis techniques [*Kumar et al.*, 2007; *Antonita et al.*, 2008; *Clemesha et al.*, 2009; *Mitchell and Beldon*, 2009; *Placke et al.*, 2011]. A related study by *Vincent et al.* [2010] employed a Monte Carlo analysis of measurement capabilities assuming a conventional meteor radar beam pattern and expected radial velocity and angle-of-arrival uncertainties and concluded that accurate momentum flux estimates with such systems would likely require long averages.

[8] Our goals in this paper are to evaluate SAAMER and DrAAMER GW momentum flux measurement capabilities relative to several other conventional meteor radars in order to determine (1) what radar parameters are required to enable such measurements, (2) whether other radars can also provide credible GW momentum flux measurements in their current configurations, or (3) whether system upgrades are needed to enable these capabilities. The other radars employed for this assessment are at Socorro (SRO), New Mexico (34.1°N, 106.9°W), Bear Lake Observatory (BL), Utah (~41.9°N, 111.4°W), and Yellowknife (YKF), Canada (62.5°N, 114.3°W) (see *Hocking* [2005] and *Hocking and Kishore Kumar* [2011], respectively, for more detailed descriptions of the SRO and YKF radars). To address these goals, our paper is structured as follows. Section 2 provides a summary of the characteristics of the radars employed for this assessment and the analysis methods used to evaluate the performance of each. Test motion fields, which include mean winds, diurnal and semidiurnal tides, and/or GWs having various characteristics are described in Section 3. The performance of the five radars for the various tests employing real spatial and temporal sampling for each is described in Section 4. Section 5 summarizes our findings and discusses measurement accuracies relative to other assessments. Our conclusions are presented in Section 6.

2. Characteristics of Radars Employed for This Study

[9] We employ five different meteor radars for our assessment of GW momentum flux measurement capabilities in this study. Two of these were specifically designed intending to provide this capability (i.e., SAAMER and DrAAMER); the other three are conventional meteor radars having lower peak power and a single transmitting antenna that had not anticipated such measurements (i.e., the SKiYMET meteor radars previously installed at Socorro, NM, Bear Lake Observatory, UT, and Yellowknife, Canada; see Table 1). The relative locations of the five radars and the meteor distributions for each are shown for one day during June in Figure 1. Meteor distributions in altitude, by day throughout the month considered, and by hour throughout a composite day for each radar are shown for comparison in Figure 2. The meteor distributions in Figure 1 all exhibit nulls in the polar diagrams that arise from excluding meteors at range increments corresponding to the pulse repetition frequency (PRF) in order to exclude contamination due to ground clutter. SAAMER (TdF) and DrAAMER (KGI) use a smaller PRF, and thus have these nulls at larger spacing. The statistics in Figure 2 include meteors at zenith angles from 15 to 60° for all radars. As expected, meteor counts are significantly larger for the radars having higher power, and higher at smaller zenith angles for SAAMER and DrAAMER than

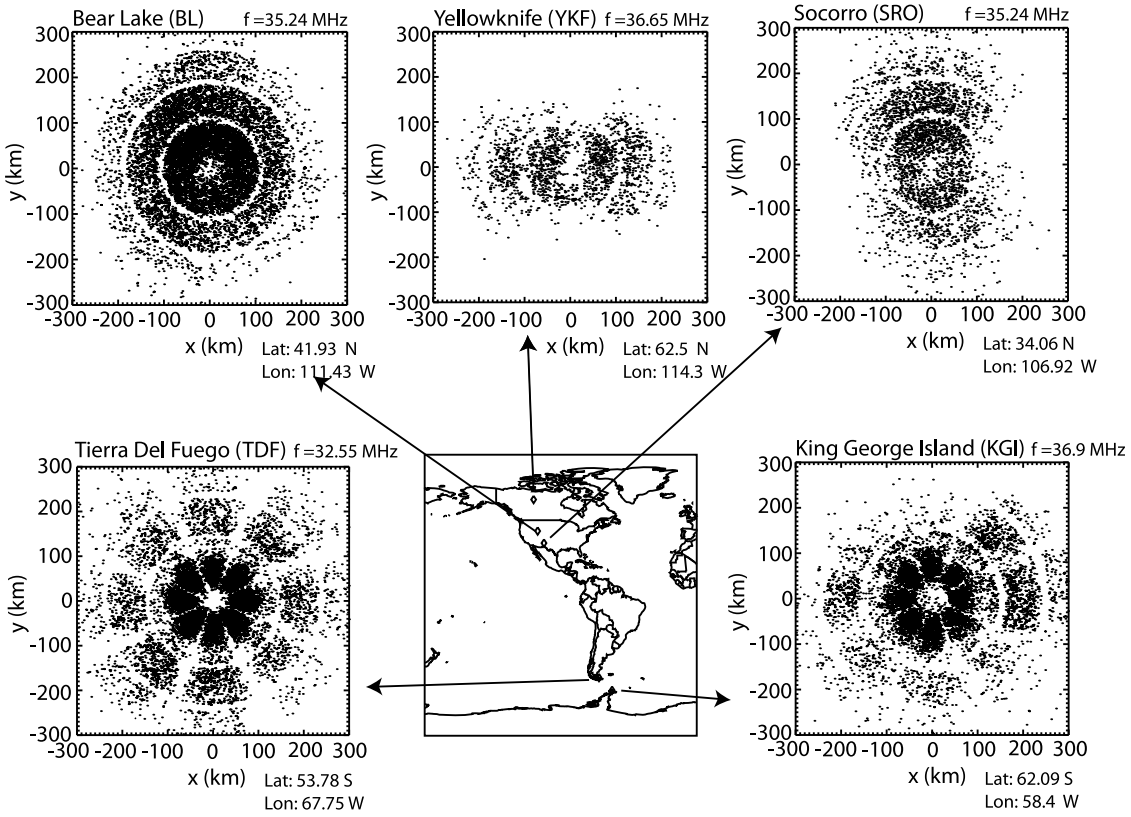

Figure 1. Daily meteor distributions illustrating the beam patterns for the five radars employed in this assessment of measurement capabilities. The radar locations and frequencies are listed in each panel. The radars at BL, TdF, and KGI use crossed Yagi antennas and have nearly symmetric beam patterns; The radars at YKF and SRO, however, use uncrossed (linearly polarized) Yagis oriented north-south and east-west, respectively, resulting in the asymmetric meteor distributions favoring east-west and north-south measurements, respectively, at those sites. Nulls at various radii in the meteor detections are due to removal of meteor detections that may have ground clutter contamination.

for the radars with single-antenna TX systems. They also vary significantly throughout the month, especially at SAAMER and DrAAMER, and exhibit large diurnal variations at all radars.

[10] The GW momentum flux measurement potential of SAAMER was previously evaluated for a number of test fields by *F10b*. Comparisons of SAAMER and DrAAMER measurements for April, May, and June of 2010 and 2011 were presented by *F11*, and suggested that DrAAMER momentum flux estimates provided a consistent picture of GW momentum fluxes accompanying strong GW sources over the Drake Passage, but did not evaluate the DrAAMER momentum flux measurement capability directly. An initial application of the method employed here was also used by *Hocking* [2005] to estimate two-monthly GW momentum fluxes by SKiYMET meteor radars at Socorro, NM and Resolute Bay, Canada. These estimates were seen to be roughly consistent with expected values, but were not evaluated in detail. A systematic evaluation of the relative momentum flux measurement potential of these various radars with specific test fields has not been performed. This is the goal here, and the characteristics of the five radars are described for comparison in Table 1. We employ meteor distributions obtained during June 2011 for KGI and TdF, June 2010 for SRO and BL, and June 2009 for YKF, for which meteor counts tend to be larger at northern than at southern latitudes. We also consider only radial velocities at zenith angles between 15 and 60° in order to avoid significant errors in mean and tidal winds and GW momentum fluxes due to measurement uncertainties (see further discussion in our error analysis in Section 5 below).

3. Specification of Test Motion Fields

[11] We showed in *F10b* that the SAAMER beam pattern and meteor counts enable relatively high-precision measurements of mean winds and tides over fairly short intervals, and that GW momentum fluxes can be estimated with reasonable accuracies where meteor counts are high, even when the large- and small-scale motion field is variable on multiple time scales. The first measurements over DrAAMER and comparisons with those over SAAMER by *F11* suggest that the same can likely be said for DrAAMER. Here we repeat the tests previously applied to SAAMER for DrAAMER and the three conventional meteor radars at Socorro, MN, Bear Lake Observatory, UT, and Yellowknife, Canada in order to evaluate DrAAMER capabilities more completely and determine whether, and under what conditions, useful GW momentum flux measurements may also be possible with the other conventional meteor radars.

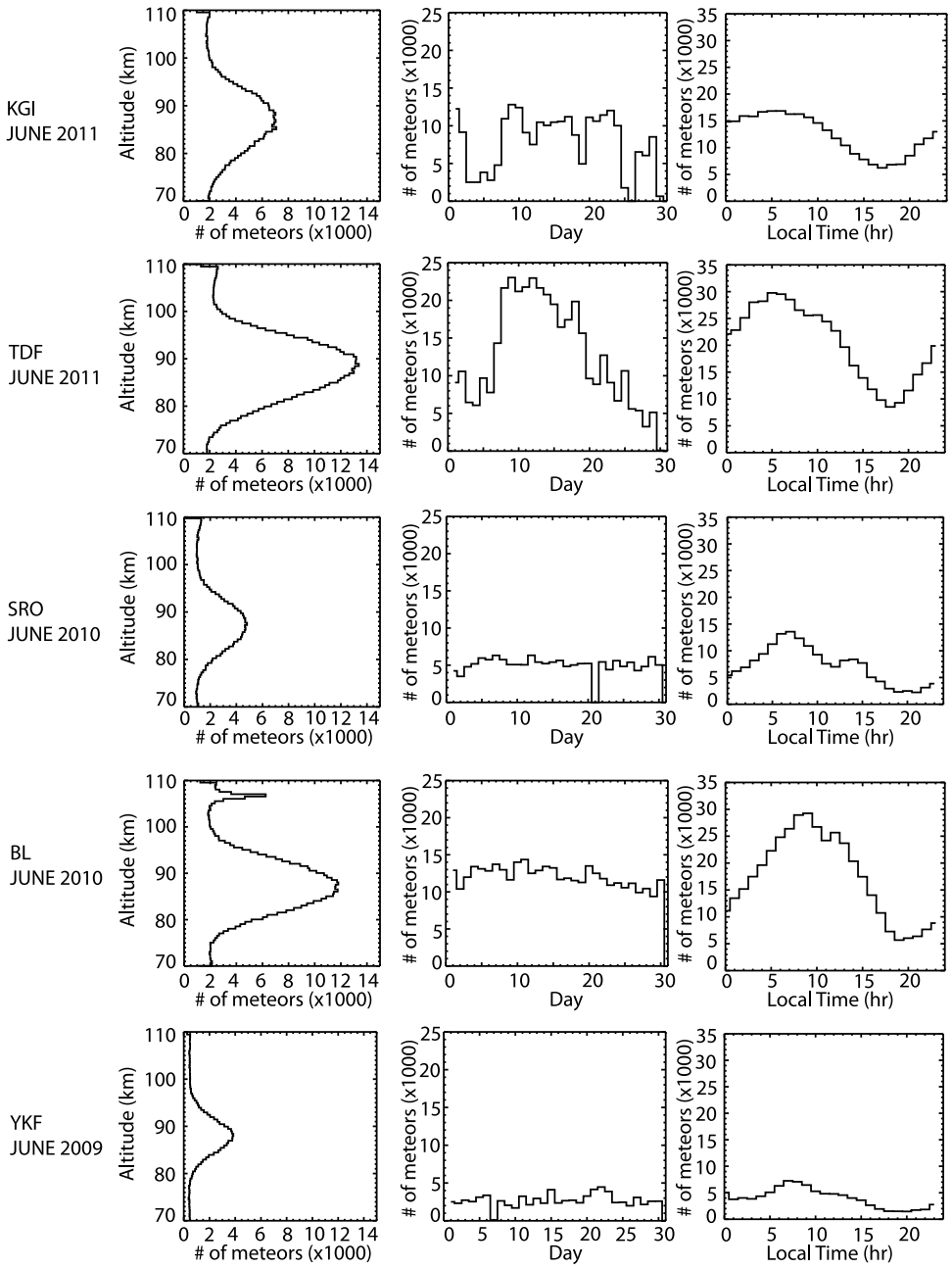

Figure 2. Accepted meteors employed for mean and tidal wind and momentum flux estimates for each radar (labeled at left). Meteor distributions are shown as (left) monthly counts in each 500 m range bin, (middle) counts per day, and (right) counts per hour for a composite day. These statistics include meteors at zenith angles between 15 and 60° for all radars examined here.

[12] Following *F10b*, we employ real meteor spatial and temporal distributions observed by SAAMER, DrAAMER, and the three other meteor radars during various months to evaluate the measurement capabilities of each. Radial velocities at each meteor location and time for each radar and each month assessed are specified by each of seven test velocity fields. Each test field includes superposed mean, tidal, and/or GW velocity fields with constant and/or spatially and temporally variable tidal and GW amplitudes that are intended to be representative of the scales, amplitudes, and momentum fluxes in the MLT over SAAMER and DrAAMER. Mean, tidal, and GW parameters defining these motion fields for each case are listed in Table 2. The test fields are those employed by *F10b*, range from highly idealized and stationary to spatially and temporally modulated at large and small scales, and have the following components:

$$\begin{aligned} U(x,y,z,t) = {} & U_M + U_D(z,t)\sin(2\pi t/T_D) + U_{SD}(z,t)\sin(2\pi t/T_{SD}) \\ & + U_{GW1}(x,y,z,t)\sin(k_1 x + l_1 y + m_1 z - 2\pi t/T_{GW1}) \\ & + U_{GW2}(x,y,z,t)\sin(k_2 x + l_2 y + m_2 z - 2\pi t/T_{GW2}) \\ & + U_{GW3}(x,y,z,t)\sin(k_3 x + m_3 z) \end{aligned} \quad (1)$$

Table 2. Mean, Tidal, and GW Parameters Used for Test Cases Evaluating Radar Measurement Capabilities Employing Real Meteor Distributions and Test Motion Fields[a]

Parameter	Case 1	Case 2	Case 3	Case 4	Case 5	Case 6	Case 7
U_M, V_M	20, 10	0, 0	0, 0	20, 10	40, −20	−20, −10	−20, −10
U_D, V_D	10, 10	0, 0	0, 0	10, 10	20, 20	10, 10	10, 10
U_{SD}, V_{SD}	50, 50	0, 0	0, 0	50, 50	$20 + 2(z - 80)\sin^2(\pi t/T_M)$	50, 50	50, 50
U_{GW1}	10	20	20	10	$20\ \mathrm{abs}[\sin(2\pi t/T_M)] * \sin(2\pi t/T_{SD})$	$40F_6(t)$	$30F_7(t)$
V_{GW1}	0	0	0	0	0	0	$30F_7(t)$
W_{GW1}	5	5	−10	5	$-10\ \mathrm{abs}[\sin(2\pi t/T_M)] * \mathrm{abs}[\sin(2\pi t/T_{SD})]$	$20F_6$ (t)	$10F_7$ (t)
k_1	$2\pi/50$	$2\pi/50$	$2\pi/30$	$2\pi/50$	$2\pi/50$	$2\pi/50$	$2\pi/40$
l_1	0	0	0	0	0	0	$2\pi/40$
m_1	0	$2\pi/15$	0	0	0	$2\pi/15$	$2\pi/15$
T_{GW1}	20	∞	∞	20	20	20	20
U_{GW2}	0	–	0	0	0	0	$30G_7(t)$
V_{GW2}	20		10	20	$20\ \mathrm{abs}[\sin(2\pi t/T_M)] * \cos(2\pi t/T_{SD})$	$30G_6$ (t)	$-30G_7(t)$
W_{GW2}	2		2	2	$5\ \mathrm{abs}[\sin(2\pi t/T_M)] * \mathrm{abs}[\cos(2\pi t/T_{SD})]$	$10G_6$ (t)	$20G_7(t)$
k_2	0		0	0	0	0	$2\pi/50$
l_2	$2\pi/100$		$2\pi/40$	$2\pi/100$	$2\pi/100$	$2\pi/100$	$2\pi/50$
m_2	0		0	0	0	$2\pi/20$	$2\pi/20$
T_{GW2}	30		∞	30	30	30	15
U_{GW3}	–	–	–	20	20	–	–
W_{GW3}				−10	−10		
k_3				$2\pi/30$	$2\pi/30$		
m_3				0	0		
V_{GW4}	–	–	–	10	10	–	–
W_{GW4}				2	2		
l_4				$2\pi/40$	$2\pi/40$		
m_4				0	0		
$\langle u'w' \rangle_m$	25	50	−100	−75	−100	50	75
$\langle v'w' \rangle_m$	20	0	10	30	10	25	−25

[a]Mean GW momentum fluxes for each case are shown at the bottom. Units for velocities, wave numbers, and periods are ms^{-1}, km^{-1}, and min, and T_M = 10 days and T_{SD} = 12 h. GWs in Case 6 are modulated by amplitude functions $F_6(t) = 1$ (t = 0–3 h + 21R_1 hr) and $F_6(t) = 0$ otherwise, and $G_6(t) = 1$ (t = 0–4 h + 20R_2 hr) and $G_6(t) = 0$ otherwise, with R_1 and R_2 random variables between 0 and 1 chosen separately for each of the 30 days of the test month. GWs in Case 7 are modulated by amplitude functions $F_7(t) = 1$ (t = 0–2 and 8–10 h + 14R_3 hr) and $F_7(t) = 0$ otherwise, and $G_7(t) = 1$ (t = 0–1 h and 6–7 h and 10–11 h and 19–20 h + 4R_3 hr) and $G_7(t) = 0$ otherwise, with R_3 and R_4 random variables between 0 and 1 as above.

$$\begin{aligned} V(x,y,z,t) = {} & V_M - V_D(z,t)\cos(2\pi t/T_D) - V_{SD}(z,t)\cos(2\pi t/T_{SD}) \\ & + V_{GW1}(x,y,z,t)\sin(k_1 x + l_1 y + m_1 z - 2\pi t/T_{GW1}) \\ & + V_{GW2}(x,y,z,t)\sin(k_2 x + l_2 y + m_2 z - 2\pi t/T_{GW2}) \\ & + V_{GW4}(x,y,z,t)\sin(l_4 y + m_4 z) \end{aligned} \quad (2)$$

$$\begin{aligned} W(x,y,z,t) = {} & W_{GW1}(x,y,z,t)\sin(k_1 x + m_1 z - 2\pi t/T_{GW1}) \\ & + W_{GW2}(x,y,z,t)\sin(k_2 x + l_2 y + m_2 z - 2\pi t/T_{GW2}) \\ & + W_{GW3}(x,y,z,t)\sin(k_3 x + m_3 z) \\ & + W_{GW4}(x,y,z,t)\sin(l_4 y + m_4 z) \end{aligned} \quad (3)$$

[13] Note that we employ the same test cases defined by *F10b*, but these equations (1)–(3) correct several typos appearing in the equations presented in *F10b*.

[14] Each test field includes some or all of the following components: (1) zonal and meridional mean winds, U_M and V_M, (2) diurnal and semidiurnal tides having zonal and meridional amplitudes of (U_D, V_D) and (U_{SD}, V_{SD}) assumed to rotate counterclockwise with time (assuming a southern hemisphere location), and which may have either constant or varying amplitudes with increasing altitude, (3) traveling GWs (GWs 1 and 2) having amplitudes (U_{GW}, V_{GW}, W_{GW}), zonal, meridional, or oblique propagation, spatial and temporal variability, correlated horizontal and vertical motions, and constant or variable momentum fluxes, and (4) stationary mountain waves (GWs 3 and 4) having zonal and meridional propagation, only spatial variability, correlated horizontal and vertical motions, and constant momentum fluxes.

[15] In each case, the test field amplitudes were chosen to correspond roughly to measured values over SAAMER and DrAAMER on TdF and KGI, which include large semidiurnal tides and GW momentum fluxes [*F10a*, *F10b*, *F11*]. Large semidiurnal tide amplitudes at these sites are consistent with expectations of the most recent version of the Global-Scale Wave Model (GSWM-09) [*Zhang et al.*, 2010a, 2010b, *F11*]. Large GW momentum fluxes are suggested by the major global hot spot of GW activity in the stratosphere and lower mesosphere centered over the Southern Andes, Drake Passage, and Antarctic Peninsula [*F10a*, and references therein].

4. Evaluation of Radar Measurement Capabilities

[16] We describe here the performance of each of the five radars for the seven test cases described above. Mean winds, diurnal and semidiurnal tidal amplitudes, and GWs having prescribed spatial and/or temporal variability and momentum fluxes propagating zonally, meridionally, or at other azimuths are defined by equations (1)–(3) for the seven cases listed in Table 2. Specified and recovered (i.e., the velocity fields inferred from our S-transform tidal fits and the Hocking statistical analysis) profiles of the mean winds, diurnal and semidiurnal tides, and GWs momentum fluxes, and their daily and composite-day hourly variability, where appropriate, are discussed separately for each case below.

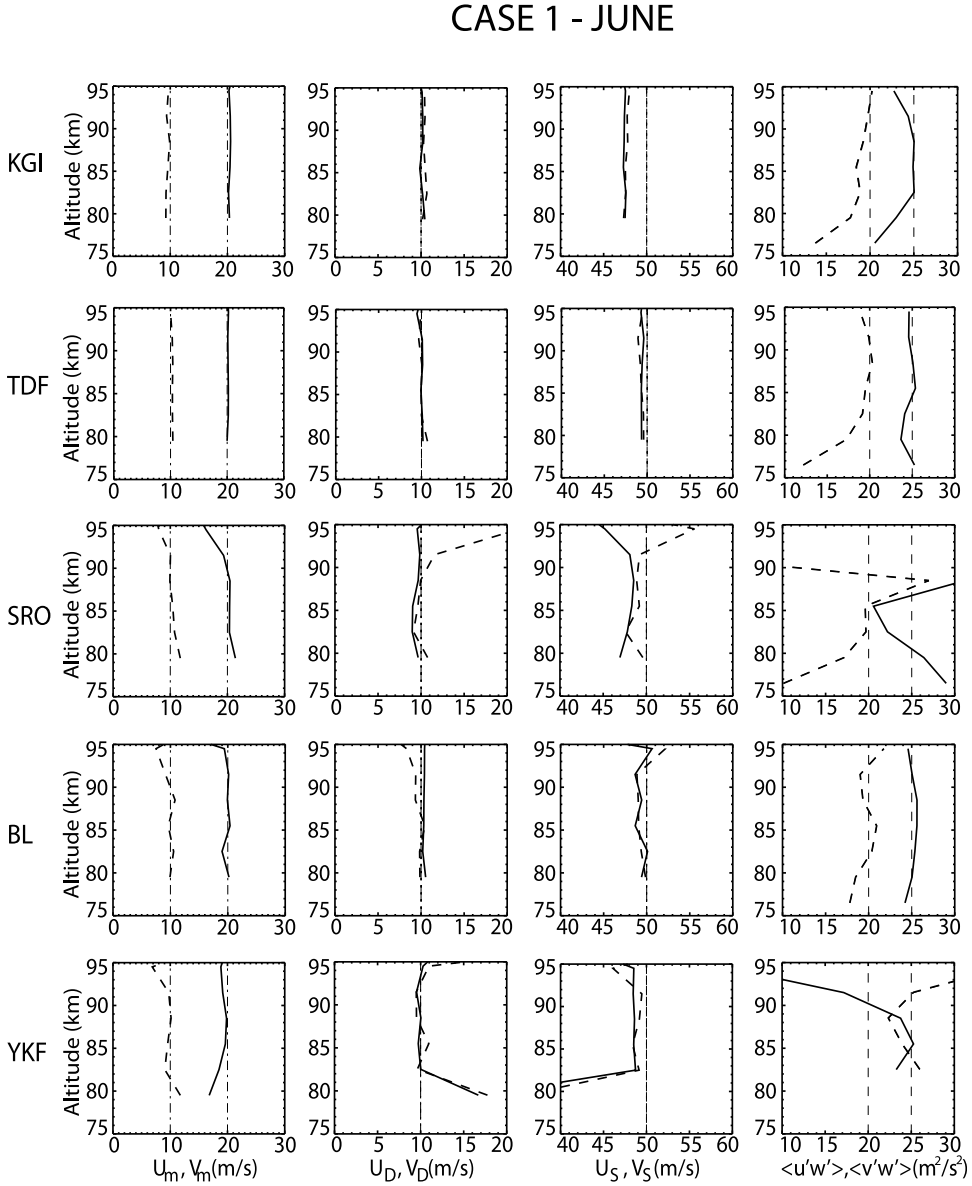

Figure 3. Monthly mean (first column) winds, (second column) diurnal tide amplitudes, (third column) semidiurnal tide amplitudes, and (fourth column) GW momentum fluxes for Case 1. Solid and dashed lines denote zonal and meridional profiles and the radars are designated at the left of each row. Vertical dashed lines show specified values.

4.1. Case 1

[17] Specified fields, and those recovered using observed meteor distributions in space and time for each radar for June 2009, 2010, or 2011 as described above, are shown as monthly means for Case 1 in Figure 3. In this case, tides have only temporal variations and GWs have only horizontal variations, with 50 and 100 km wavelengths in the zonal and meridional motions, respectively (see Table 2).

[18] As seen in Figure 3, agreement between specified and recovered fields is highly variable among the five radars. As might be expected based on meteor counts, mean winds and diurnal and semidiurnal tidal amplitudes are recovered quite well at KGI, TdF, and BL. Mean winds and diurnal tide amplitudes are recovered within a few percent at each of these sites, with slightly greater uncertainties at BL than at the other two. Semidiurnal tide amplitudes are systematically less than specified at all three sites, but only by ~2–3% at TdF and BL, and by ~5% at KGI. Mean winds and tidal amplitudes exhibit similar tendencies and accuracies at SRO and YKF at the central altitudes, but increasing errors at the lowest and highest altitudes where meteor counts are small.

[19] GW momentum flux estimates at KGI, TdF, and BL are likewise accurate within ~10%, except at KGI and TdF below 79.5 km. In contrast, SRO and YKF exhibit errors of ~20% or larger at intermediate altitudes, again with larger errors where meteor counts are small.

4.2. Case 2

[20] Case 2 includes no mean winds or tides and only a zonal stationary GW with prescribed horizontal and vertical

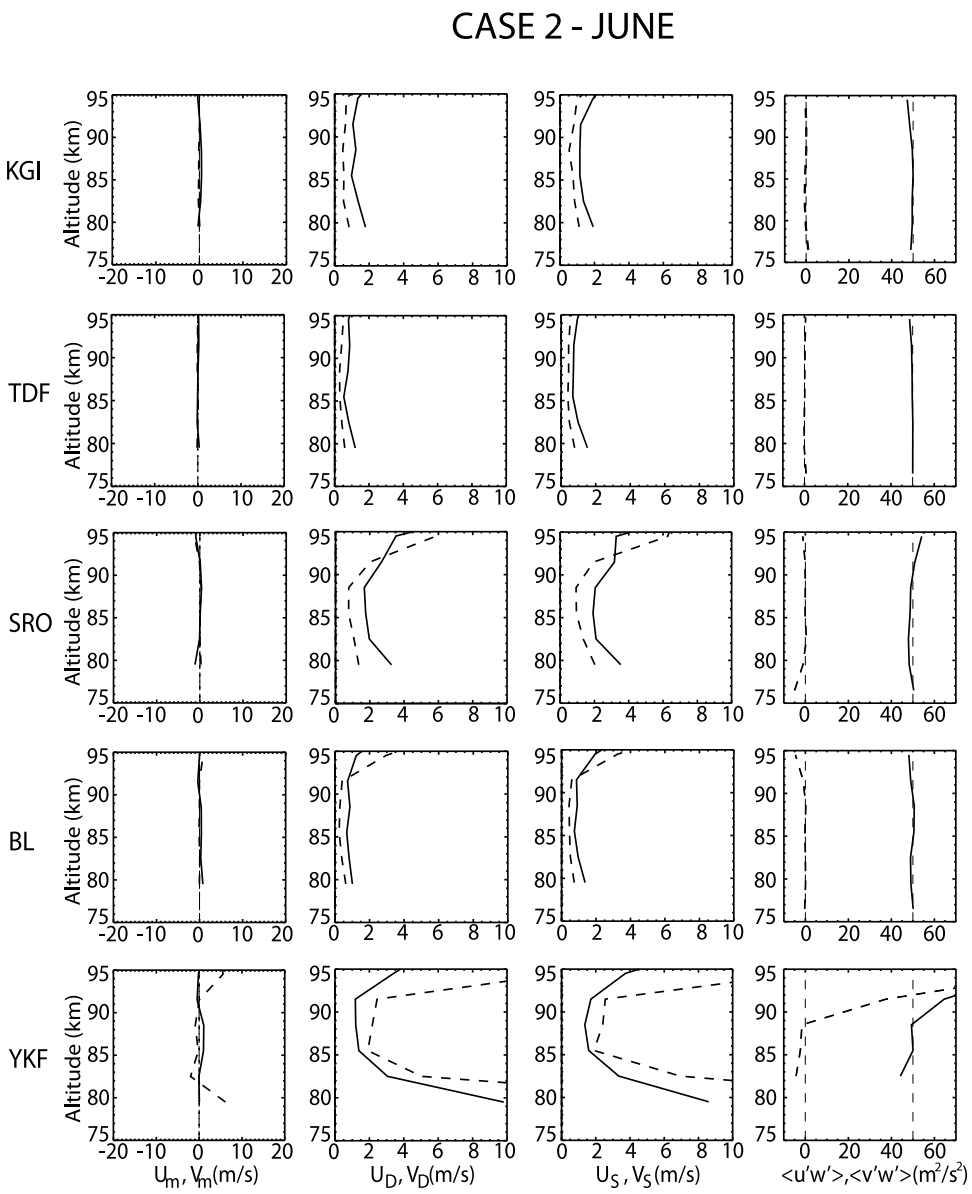

Figure 4. Same as Figure 3 but for Case 2.

phase variations with wavelengths of 50 and 15 km (not physical, but simple, see Table 2). Referring to Figure 4, we see that, as in Case 1, the recovered mean and tidal motions are quite accurate at KGI, TdF, and BL, typically within $\sim$2 ms^{-1} or better, except for the tidal amplitudes at BL above $\sim$92 km. Estimates at SRO and YKF are slightly less accurate, within $\sim$5 ms^{-1}, but nevertheless quite reasonable, except at the highest and lowest altitudes, especially at YKF.

[21] Unlike Case 1, all the radars except YKF provided accurate estimates of GW momentum fluxes in this case, with the largest departures of only $\sim$5 m^2 s^{-2} at the highest and lowest altitudes shown. However, meteor counts at YKF were apparently too small to yield adequate statistics, except at the central altitudes having the highest meteor counts, from 82.5 to 88.5 km. The significant differences in the accuracies of the GW momentum fluxes at all sites and in the mean wind and tidal amplitudes between Cases 1 and 2 suggest a strong influence of large and variable winds on the quantification of GW momentum fluxes, even for persistent and well-defined GWs. These influences will be quantified further below and discussed in some detail in Section 5.

4.3. Case 3

[22] Case 3 considers a motion field varying from that of Case 2 only in having two orthogonal GWs, each of which has no phase variation in altitude or time and with the GW propagating in the zonal plane having a large vertical velocity of 10 ms^{-1} (again not physical, but simple). Results displayed in Figure 5 show that mean motions, tidal amplitudes, and GW momentum fluxes are again described well with the meteor distributions for KGI, TdF, and BL, and the mean motions and GW momentum fluxes are described reasonably at SRO and at YKF, but with increasing errors in momentum fluxes at the higher altitudes. However, tidal amplitudes now exhibit larger errors at SRO and YKF than

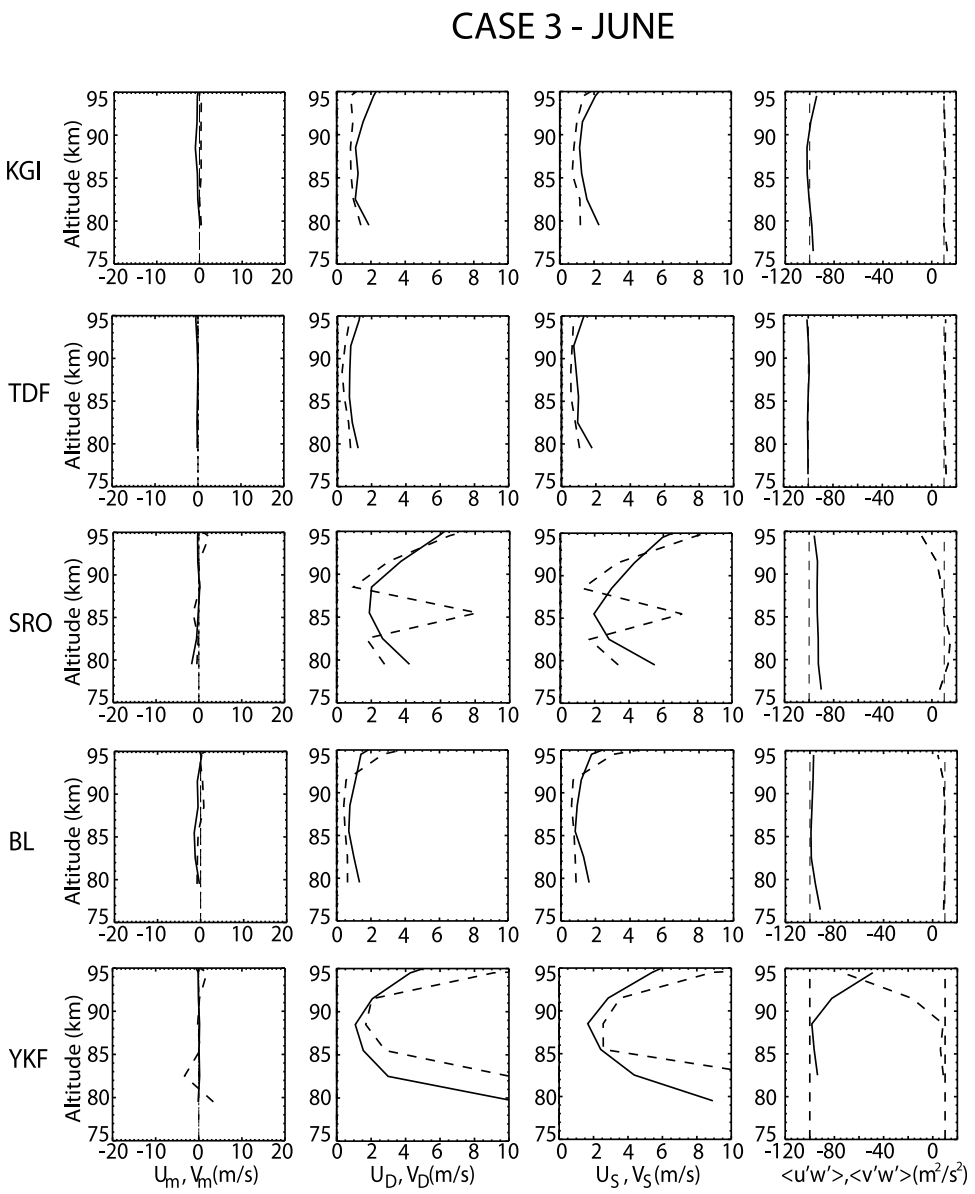

Figure 5. Same as Figure 3 but for Case 3.

seen in Case 2, with these motions reasonably defined at ~85 to 92 km at YKF and in the zonal component at SRO, but poorly defined at lower and higher altitudes at both these sites and even at central altitudes in the meridional components at SRO. This cannot be a result of insufficient sampling of the mean and tidal motions, as they are all zero. Instead, the cause appears to be the larger GW vertical velocities that are not sufficiently averaged in defining large-scale (horizontal) winds, despite the validity of the momentum flux estimates for stationary GWs at these sites (see further discussion in Section 5).

4.4. Case 4

[23] We now consider a more complex superposition of mean, tidal, and GW fields given by the sum of the mean and tidal motions in Case 1 and both stationary and propagating GWs in both the zonal and meridional planes (see Table 2). This case differs from the previous cases in that both zonal and meridional GW momentum fluxes now have contributions from stationary and propagating GWs having different spatial structures (with horizontal wavelengths of 30, 40, 50, and 100 km). Case 4 also includes both large semidiurnal tide amplitudes and GW vertical velocities that were suggested above to contribute to errors in the estimates of mean and tidal amplitudes and GW momentum fluxes. Depending on the phases of the four GWs, vertical motions may be ~15 ms^{-1} or larger in this case.

[24] Results displayed in Figure 6 show that errors in estimates of the mean winds and tidal amplitudes are comparable (and small) for Cases 1 and 4 at KGI, TdF, and BL. Semidiurnal tide amplitudes are underestimated, with the largest errors of ~5% at KGI (note the different scales in the third columns of Figures 3 and 6). As seen in Case 1, mean wind and tidal amplitude estimates at SRO and YKF for Case 4 are also reasonable at central altitudes, but exhibit

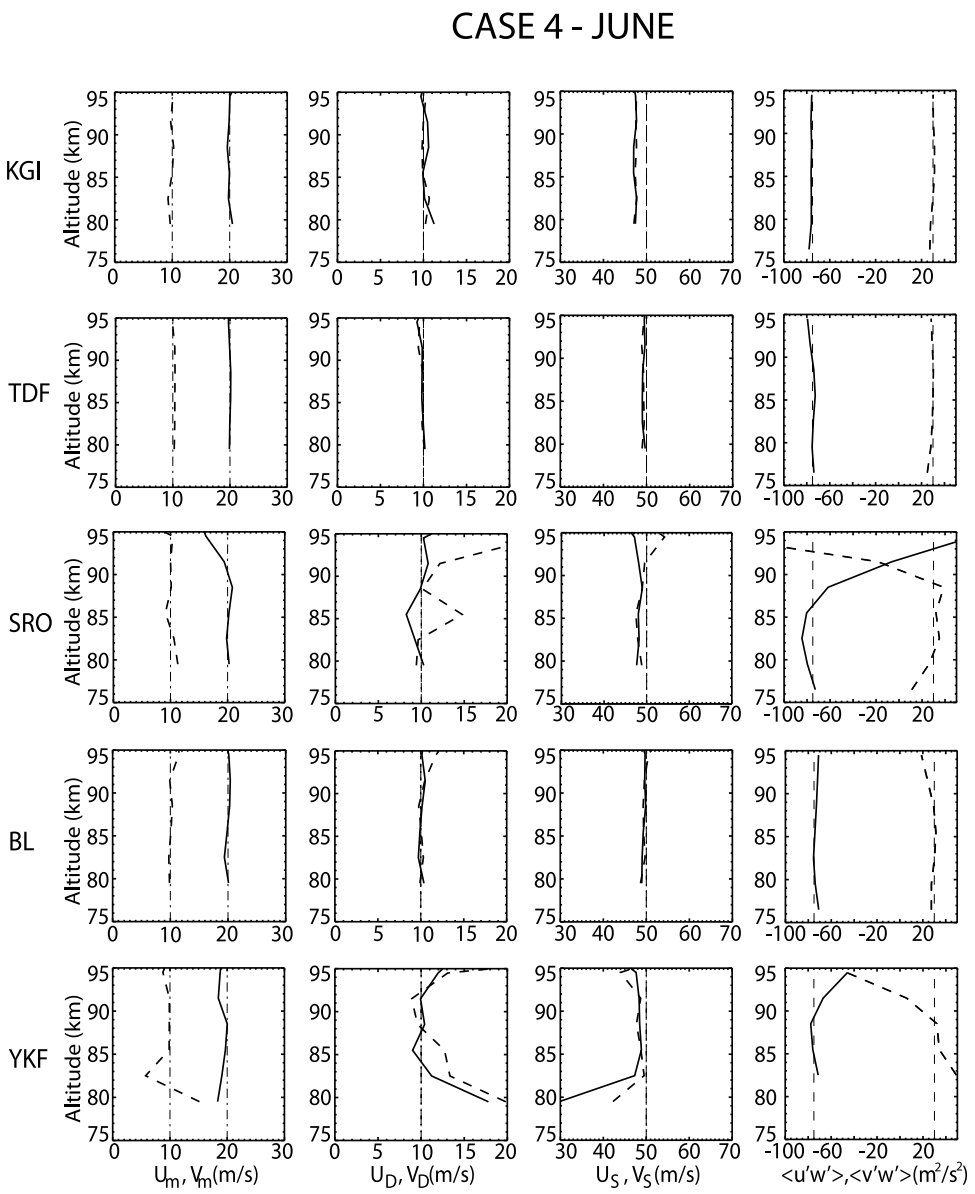

Figure 6. Same as Figure 3 but for Case 4.

greater errors at lower and/or higher altitudes and at central altitudes in the meridional diurnal tide amplitudes.

[25] Turning now to GW momentum flux estimates for Case 4, we see that these are very good at KGI, TdF, and BL, with comparable errors ($\sim$a few m^2 s^{-2}) except at the highest and lowest altitudes where they are somewhat larger. Similar estimates are also obtained at SRO and YKF at central altitudes (with errors for Case 4 of $\sim$10 m^2 s^{-2} or less), with much larger errors occurring at lower and higher altitudes. Apparently, mean winds and large tidal amplitudes do not prevent accurate estimates of GW momentum fluxes when meteor counts are sufficiently high and GWs are sufficiently sustained (whether stationary or propagating) to enable sampling of all phases throughout the month. Large GW amplitudes (especially vertical velocities), however, do cause errors in estimates of means winds and tidal amplitudes where meteor counts are not sufficiently high.

4.5. Case 5

[26] Case 5 explores a superposition of larger mean winds, a larger, but constant, diurnal tide, a semidiurnal tide that exhibits both a 10-day amplitude modulation and amplitude growth with altitude, and four superposed GWs. The latter include (1) stationary GWs having zonal and meridional orientations, constant amplitudes and momentum fluxes, and horizontal wavelengths of 30 and 40 km and (2) propagating GWs having zonal and meridional orientations, horizontal wavelengths of 50 and 100 km, respectively, and amplitude (and momentum flux) modulation by, and anti-correlations with, the semidiurnal tide amplitudes.

[27] Results for Case 5 are displayed in four formats. Figure 7 shows monthly mean profiles of mean winds, tidal amplitudes, and GW momentum fluxes similar to Cases 1 to 4 above. Figure 8 displays daily estimates of mean winds and diurnal tide amplitudes throughout the month in the

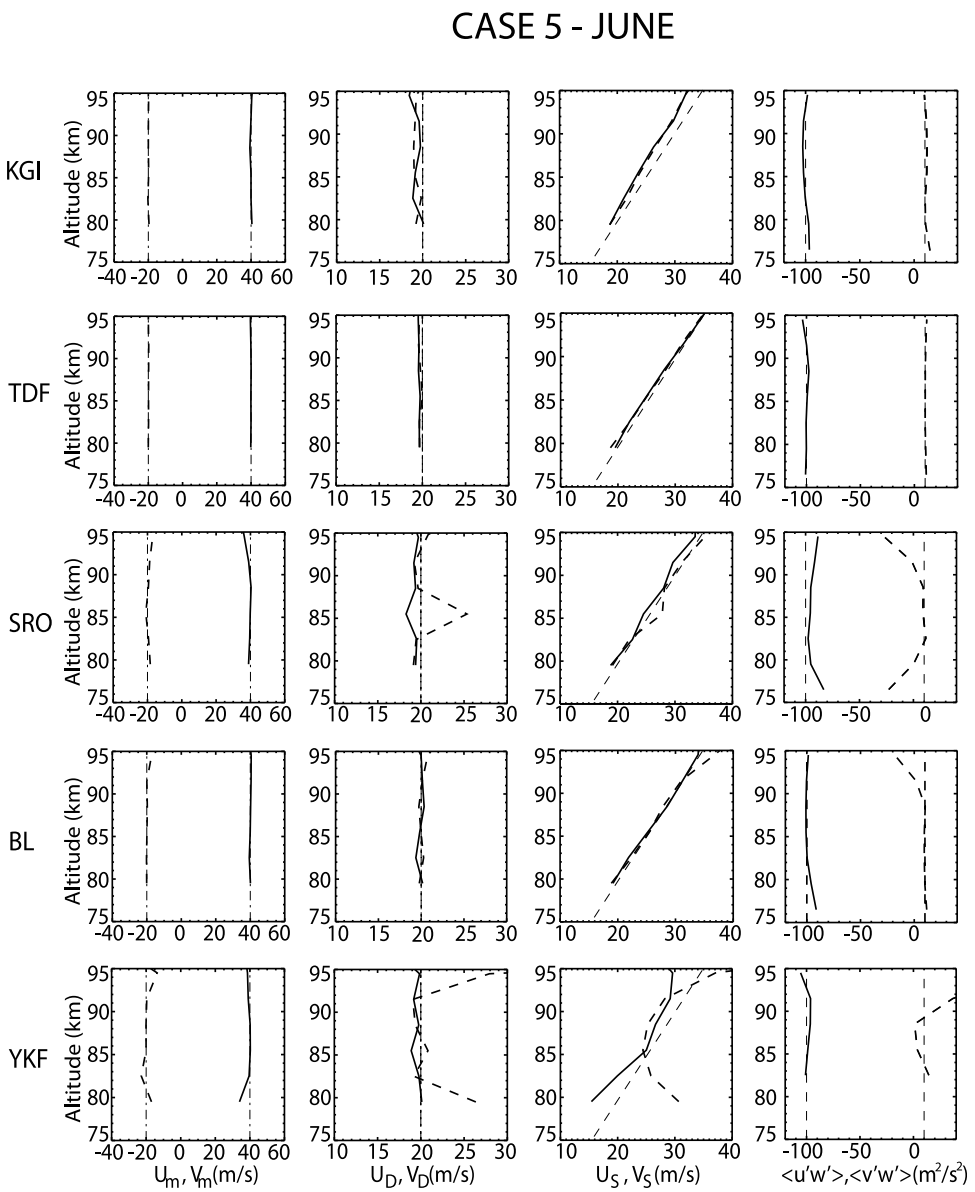

Figure 7. Same as Figure 3 but for Case 5.

presence of variable semidiurnal tide and GW amplitudes. Figure 9 compares daily estimates of semidiurnal tide amplitudes with the specified variations. Hourly estimates of GW momentum fluxes throughout the composite day are compared with the specified variations in Figure 10.

[28] Results shown in Figure 7 reveal mean wind estimates (first column) that are very accurate at all radars (within $\sim$1 ms^{-1} except at the lowest and highest altitudes at SRO and YKF). Diurnal tide amplitude estimates (second column) are likewise very good at TdF, nearly as good at KGI and BL (within $\sim$1 to 2 ms^{-1}), and reasonable at central altitudes at YKF (within $\sim$2 ms^{-1}). Somewhat larger errors ($\sim$5 ms^{-1}) are again seen in the meridional diurnal amplitude at SRO. Mean semidiurnal tide amplitude estimates (third column) are seen to be very precise at TdF and BL, to exhibit slight underestimates at KGI, and to have comparable errors about the specified mean amplitudes at SRO. Larger errors are seen at YKF (as large as $\sim$5–10 ms^{-1}), but the amplitude growth with altitude is still captured at the central altitudes.

[29] Daily mean wind and diurnal tide amplitude estimates shown for Case 5 in Figure 8 are most accurate at TdF and BL (with RMS uncertainties of $\sim$1 ms^{-1} or less) and somewhat less accurate at KGI (with RMS uncertainties of $\sim$2 ms^{-1}), except at the lowest altitude at KGI and the lowest and highest altitudes at BL where meteor counts are small. Daily mean estimates are considerably less accurate at SRO and YKF due to the significantly smaller meteor counts at all altitudes and the asymmetric meteor distributions seen in Figure 1. RMS errors of these estimates range from a few ms^{-1} for the zonal components at central altitudes at SRO to $\sim$100% or greater uncertainties at YKF that render the latter useless in defining day-to-day variability in these quantities.

[30] Estimates of semidiurnal tide zonal and meridional amplitudes for each day in Case 5 at 3-km altitude intervals

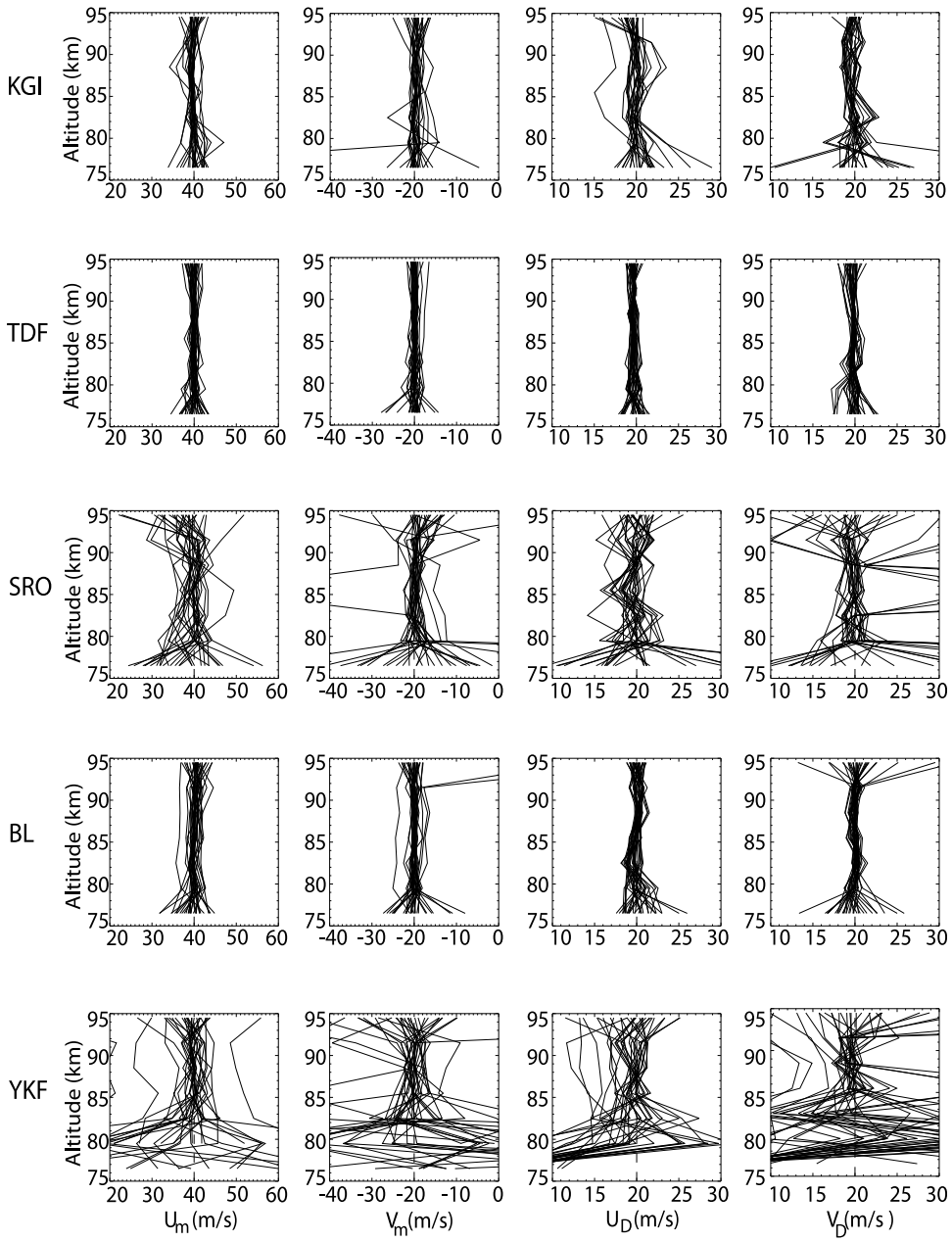

Figure 8. Daily (first column) zonal mean winds, (second column) meridional mean winds, (third column) zonal diurnal tide amplitudes, and (fourth column) meridional diurnal tide amplitudes for Case 5. Vertical dashed lines show specified values.

are displayed in the left and right panels of Figure 9. These estimates are seen to be in close agreement with the specified values (dashed lines) at all but the lowest altitude at TdF and the lowest and highest altitudes for KGI and BL. Estimates at SRO and YKF, in contrast, are reasonably accurate at the central four altitudes, apart from sporadic departures of $\sim$20 to 60 ms^{-1} at these altitudes, primarily at YKF and in the meridional component at SRO.

[31] Hourly estimates of zonal and meridional GW momentum fluxes for the Case 5 composite day at 3-km altitude intervals are shown in Figures 10 (left) and 10 (right). These are seen to be close approximations to the specified values at TdF for all but the lowest and highest altitudes, and even to follow the semidiurnal momentum flux modulations at these altitudes, but with larger uncertainties. The results for KGI and BL are comparable and also very good, but exhibit somewhat larger fluctuations about the specified values than seen at TdF at the central four altitudes and increasing uncertainties at KGI at 76.5, 79.5, and 97.5 km and at BL at 76.5, 94.5, and 97.5 km. Composite day hourly momentum flux estimates for SRO and YKF are seen to occasionally follow the specified semidiurnal modulation at 85.5, 88.5, and 91.5 km, but with very large uncertainties. At higher and lower altitudes, these estimates exhibit very large errors.

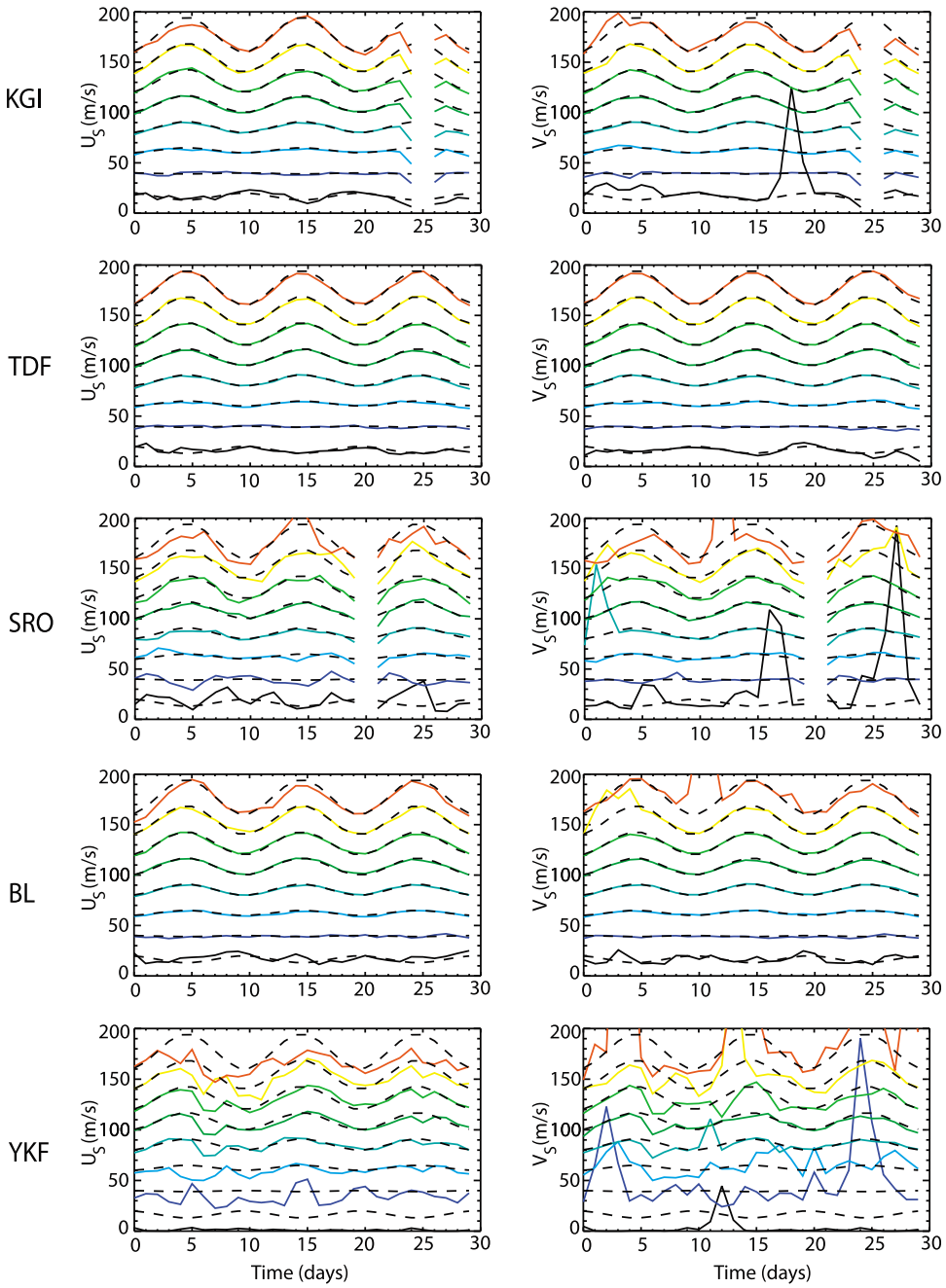

Figure 9. Daily (left) zonal and (right) meridional semidiurnal tide amplitudes for Case 5 for the five radars (labeled at the left of each row). Colored lines show measured amplitudes from (black) 76.5 to (red) 97.5 km, dashed lines show specified amplitudes.

4.6. Case 6

[32] We now compare the ability of the five radars to define mean and tidal motions and GW momentum fluxes for the motion field defined by Case 6 in Table 2. This case includes mean and tidal motions representative of higher latitudes and two transient GW packets having propagation to the east and north and that occur randomly for 3 and 4 h each day. The two GWs have zonal and meridional propagation, daily mean momentum fluxes of 50 and 25 m^2 s^{-2}, and periods of 20 and 30 min, respectively. Both also have horizontal and vertical phase variations with wavelengths given in Table 2. Inferred monthly mean winds, tidal amplitudes, and GW momentum fluxes obtained with each radar are shown in Figure 11. Hourly estimates of zonal and meridional GW momentum fluxes for a Case 6 composite day at 3-km altitude intervals are shown in the left and right panels of Figure 12. Note here that the composite day momentum flux variations are different for each radar in each component. Case 6 differs from Cases 1 and 4 in having (1) different, but comparable, mean motions, (2) stochastic rather than uniform (and stationary) GWs, and (3) vertical phase variations of the GWs.

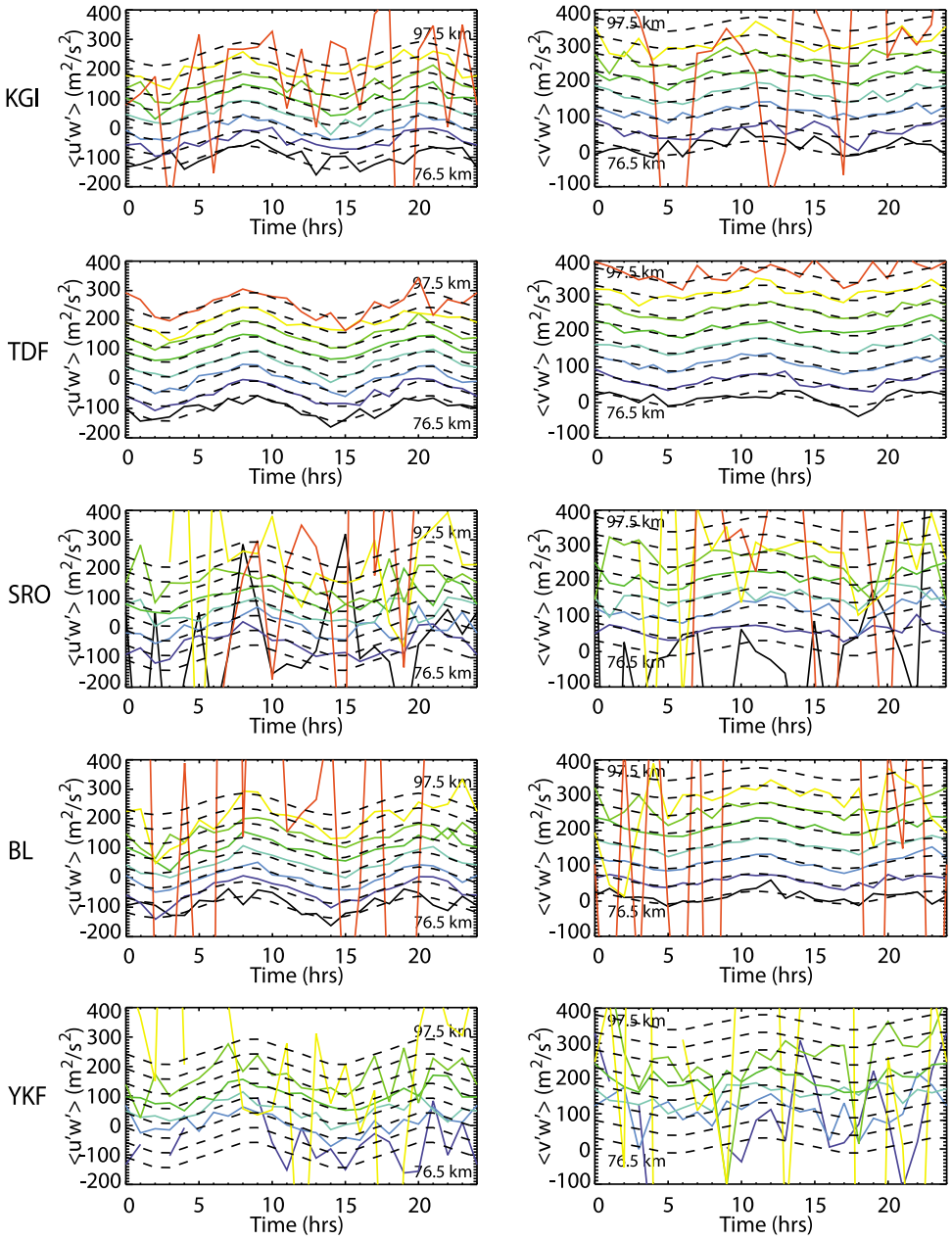

Figure 10. Hourly (left) zonal and (right) meridional GW momentum fluxes for Case 5 for a composite day for the five radars (labeled as in Figure 9). Colored lines show measured amplitudes from (black) 76.5 to (red) 97.5 km. Dashed lines show specified amplitudes.

[33] Monthly estimates of mean winds and tidal amplitudes shown in the first through third columns of Figure 11 have accuracies and biases that are very similar to those seen previously in Cases 1 and 4. Mean wind and diurnal tide amplitude estimates are again very accurate at TdF and nearly as accurate at KGI and BL. Somewhat greater uncertainties are observed at SRO and YKF, but even these are not larger than $\sim$2 ms^{-1} except at the lowest and highest altitudes. Semidiurnal tide amplitude estimates are also nearly identical to those obtained in Cases 1 and 4. Amplitudes are again under-estimated by $\sim$5% at KGI, SRO, and YKF, and by $\sim$2% at TdF and BL. The similar accuracies achieved in these three cases suggest that the greater intermittency of the larger amplitude GWs in Case 6 does not impact the ability of these radars to provide reasonably accurate definitions of the monthly mean and tidal fields.

[34] GW momentum flux estimates shown in the fourth column of Figure 11 are seen to be relatively more accurate at KGI, TdF, and BL, where uncertainties are $\sim$10% or less at central altitudes, but approach 20% at KGI and BL at the lowest and/or highest altitudes. Momentum flux estimates are also relatively accurate at SRO and YKF at the central 2 to 4 altitudes having the highest meteor counts, but exhibit large errors at lower and higher altitudes where meteor counts are low. Accuracies at KGI, TdF, and BL are comparable to those seen in Case 1 for which GW amplitudes and momentum fluxes are smaller. However, accuracies are not as good as seen in Case 4 where the zonal momentum

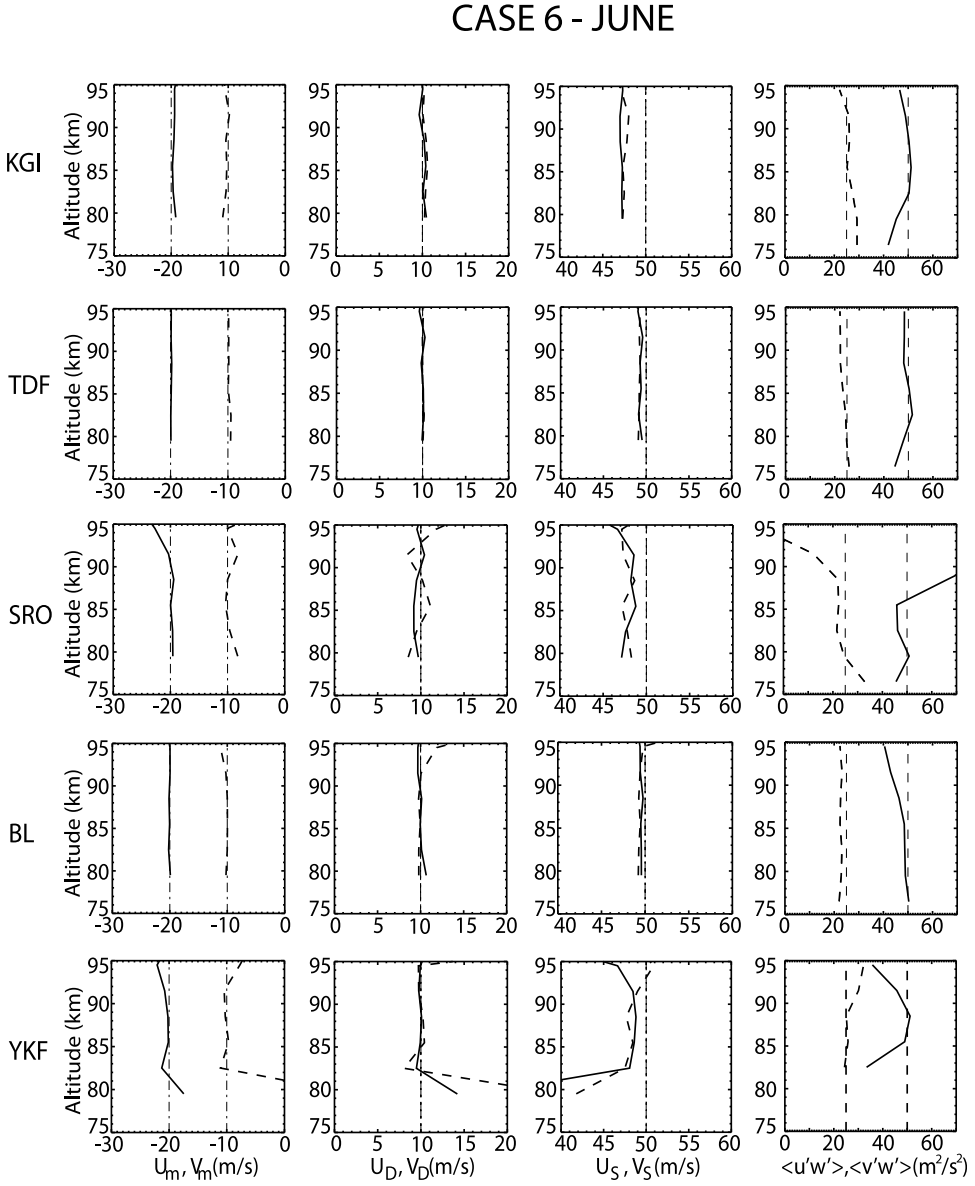

Figure 11. Same as Figure 3 but for Case 6.

flux is largely determined by the stationary, large-amplitude GW contributing the majority of the momentum flux.

[35] Diurnal variability of the composite day zonal and meridional momentum fluxes for each radar shown in Figure 12 reinforce the statements above about the monthly mean profiles. The TdF and BL radars capture the specified momentum flux distributions extremely well, but with slightly greater uncertainties at TdF at the highest altitude, at TdF and BL at the lowest altitude, and a greater loss of sensitivity at the highest altitudes at BL. Momentum flux estimates at KGI are slightly less precise than either TdF or BL at central and lower altitudes, but are somewhat better than at BL at the higher altitudes. In contrast, momentum flux estimates at SRO and YKF are only accurate at the central ~4 and 2 altitudes, respectively, and are susceptible to very large uncertainties below and above. These results suggest that high meteor counts (and more uniform sampling of the motion field) are essential in defining momentum fluxes when GWs are variable and tides achieve large amplitudes. We note that variable tidal amplitudes do not contribute significantly to these uncertainties because the variable tides are removed from each data set using the sliding S-transform procedure described by *F10b*.

[36] In order to assess whether momentum flux estimates are negatively influenced by large tidal amplitudes, we also performed the same mean, tidal, and GW momentum flux assessments for Case 6, but with zero mean winds and tidal amplitudes. This yielded (1) very accurate mean wind estimates (except at the lower altitudes at YKF), (2) diurnal and semidiurnal tide amplitude estimates of ~1 ms^{-1} at KGI, TdF, and BL and ~2 ms^{-1} at the central altitudes at SRO and YKF, and (3) momentum flux estimates comparable to or slightly more accurate than with the tides present, with the greatest improvements at SRO. Hourly estimates for the composite day without mean winds and tides are likewise

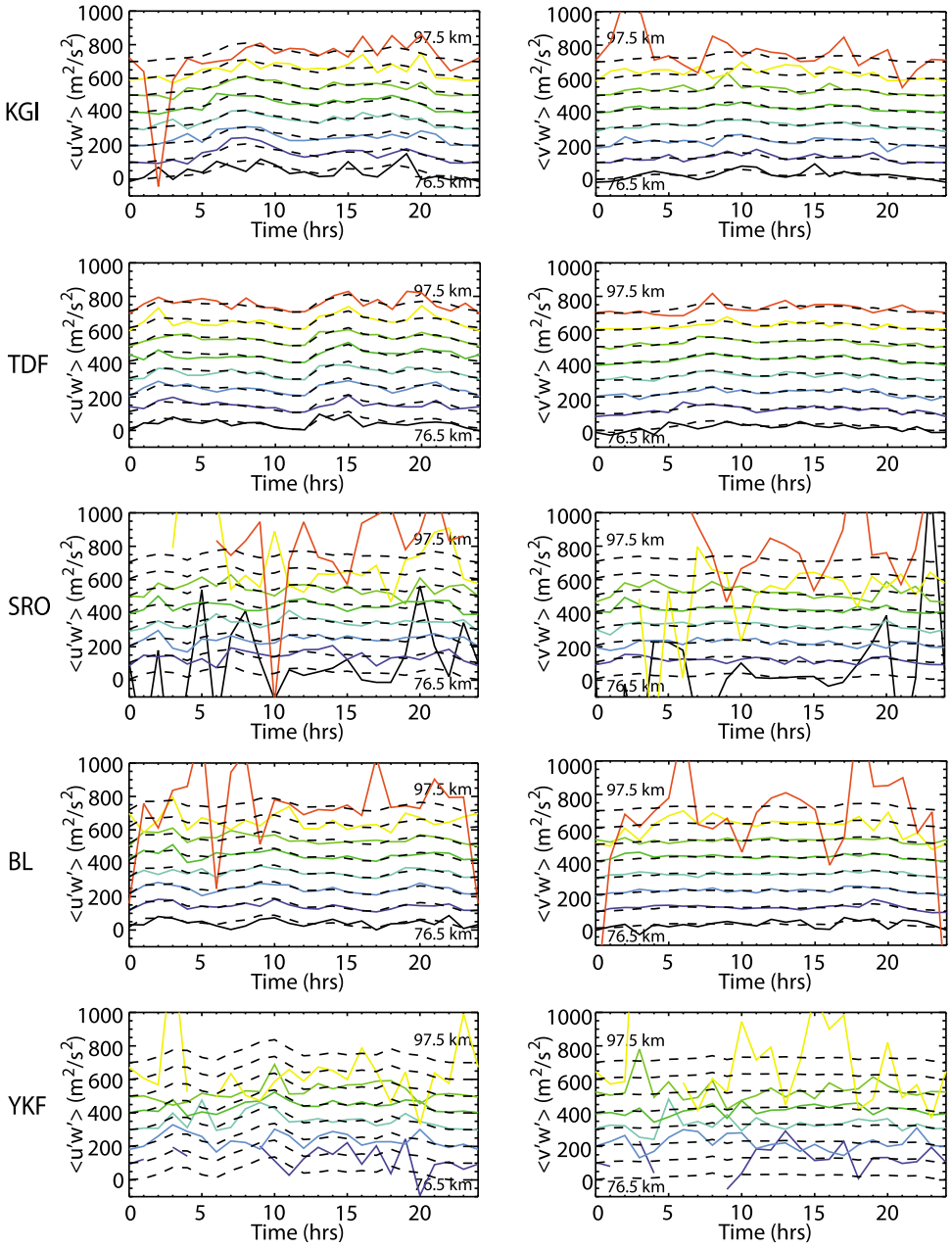

Figure 12. Same as Figure 10 but for Case 6.

of comparable accuracy to those for the full field specified for in Case 6 in Table 2.

4.7. Case 7

[37] Case 7 is very similar to Case 6, with the same mean and tidal winds, but including two intermittent large-amplitude GWs having propagation to the NE and SE. The GW propagating to the NE occurs for 2 h twice daily at random times; that propagating to the SE occurs for 1 h 3 times daily at random times. The GWs have periods of 20 and 15 min and both horizontal and vertical phase variations. Amplitudes and wavelengths of each are listed in Table 2. Together, they result in mean zonal and meridional momentum fluxes of 75 and -25 m^2 s^{-2}, respectively. Inferred monthly mean winds, tidal amplitudes, and GW momentum fluxes obtained with each radar for Case 7 are shown in Figure 13. Figure 14 shows hourly estimates of zonal and meridional GW momentum fluxes for a Case 7 composite day at 3-km altitude intervals.

[38] Monthly mean wind, tidal amplitude, and GW momentum flux estimates for Case 7 are very similar to those seen in Case 6 above. Mean wind and diurnal tide amplitude estimates are very accurate at KGI, TdF, and BL but exhibit larger errors at SRO and YKF at the highest and lowest altitudes, respectively. Semidiurnal tides are underestimated by ~5% at KGI, SRO, and YKF, and by ~2% at TdF and BL, as in Case 6. However, larger errors are seen at SRO and YKF at the highest and lowest altitudes, respectively, as seen for the mean winds and diurnal tide amplitudes. GW momentum flux estimates also exhibit

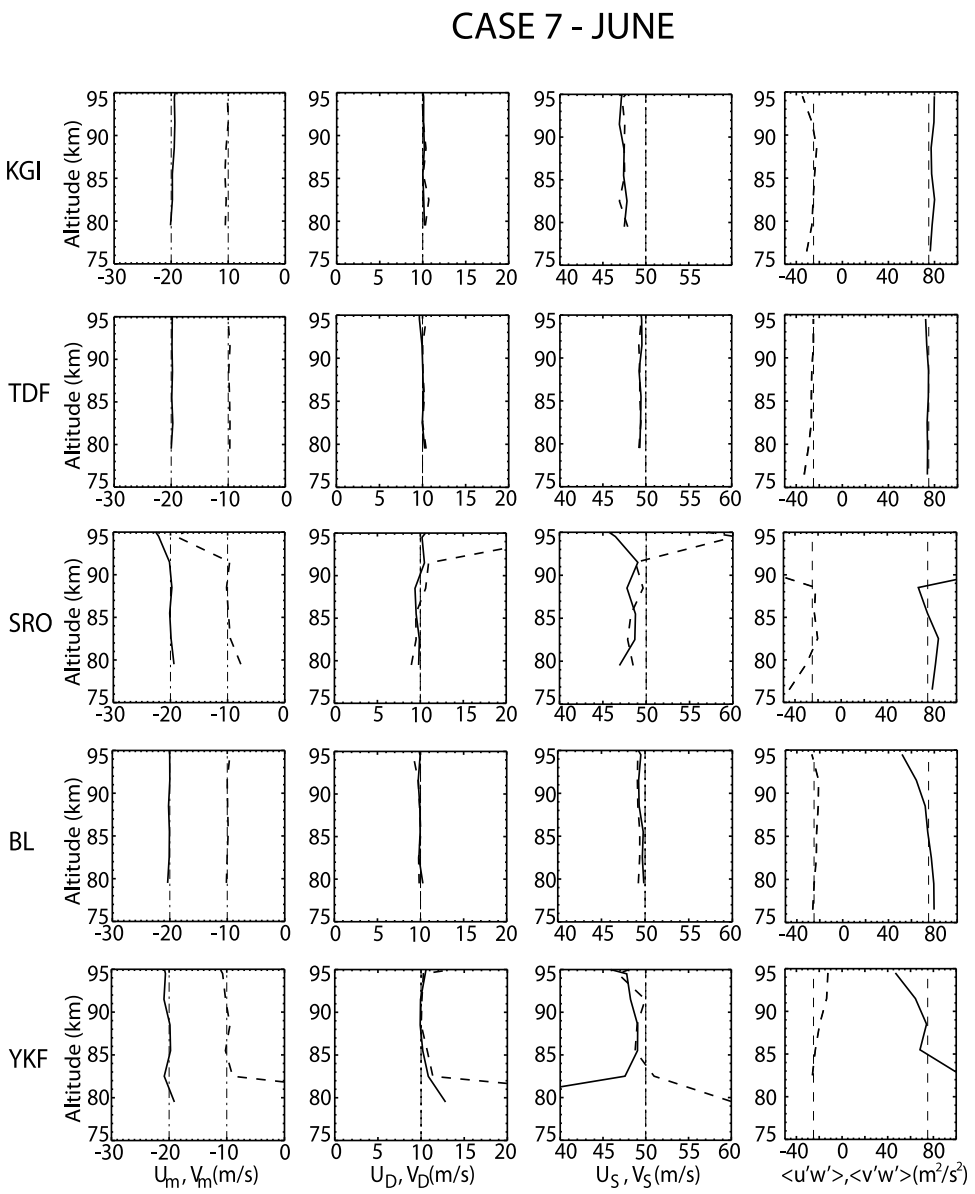

Figure 13. Same as Figure 3 but for Case 7.

comparable accuracies to those in Case 6, suggesting that GW packet duration does not have a strong influence on the ability to define these quantities. Finally, as for Case 6, we also performed these assessments with mean winds and tidal amplitudes specified to be zero. Similar to the results for Case 6, this yielded (1) extremely accurate mean wind estimates (except at the lower altitudes at YKF), (2) diurnal and semidiurnal tide amplitude estimates of ~1–2 ms^{-1} at KGI, TdF, and BL and ~2–5 ms^{-1} at the central altitudes at SRO and YKF, and (3) momentum flux estimates comparable to or slightly more accurate than with the tides present. As in Case 6, hourly estimates for the composite day without mean winds and tides are of comparable accuracy to those for the full field specified for Case 7 in Table 2.

5. Summary and Discussion

[39] We have assessed the relative measurement accuracies of meteor radars having similar frequencies (32.55 to 36.9 MHz) but different antenna configurations, peak power, and sampling modes. Our evaluation was performed with meteor distributions observed by five radars extending from 62.1°S to 62.5°N obtained during June of 2009, 2010, or 2011 for which meteor statistics tend to be better at northern than southern latitudes. Two of these radars, SAAMER on Tierra del Fuego and DrAAMER on King George Island (53.8 and 62.1°S, respectively) were specifically designed for enhanced measurement capabilities for large-scale motions and GW momentum fluxes. This was accomplished in each case with an 8-Yagi transmitting array directing power into 8 lobes centered at 35° zenith angles separated by 45° in azimuth. The other three radars are conventional meteor radars at northern latitudes (see Figure 1). Our purpose was to determine the relative abilities of different meteor radar configurations to recover specified mean winds, diurnal and semidiurnal tide amplitudes, and GW momentum fluxes.

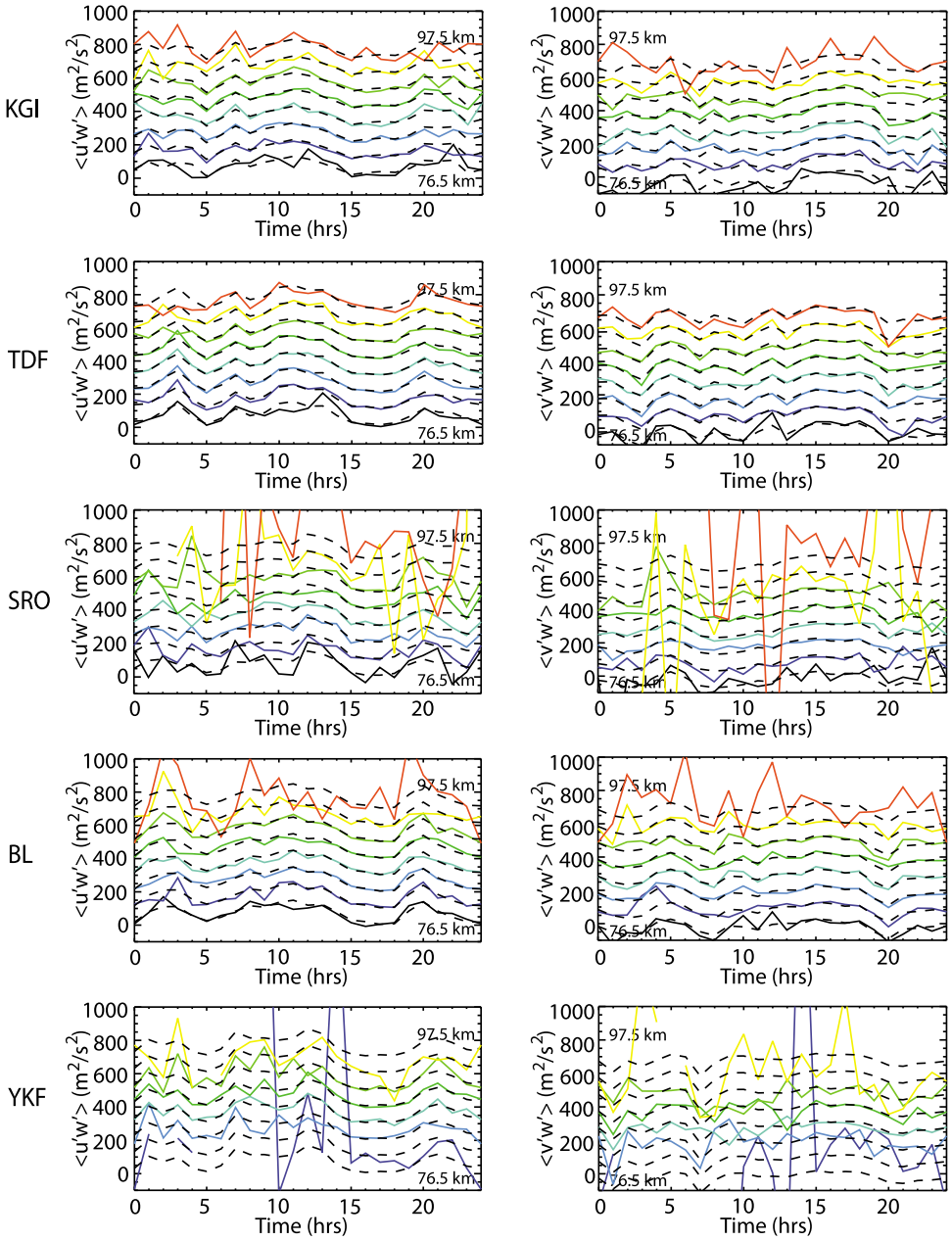

Figure 14. Same as Figure 10 but for Case 7.

[40] Seven test motion fields included various superpositions of constant mean winds, constant and/or variable tidal amplitudes, and GWs having varying amplitudes, momentum fluxes, scales, periods, propagation directions, and intermittencies. We did not examine variable tidal phases, expecting that our use of a sliding S-transform would remove phase variations as effectively as amplitude variations. The test fields were sampled according to the observed meteor distributions throughout the month for each radar assuming no radial velocity, range, or angular uncertainties in the measurements. Only meteors at zenith angles between 15 and 60° were used, due to the large altitude uncertainties accompanying ~1° zenith angle uncertainties in angle-of-arrival estimates at larger zenith angles. The various fields were estimated in 3-km altitude bins (centered from 76.5 to 94.5 km) using the method described by *F10b*, in which mean winds and tidal amplitudes are determined by S-transform fits and removed from each radial velocity distribution before application of the *Hocking* [2005] method. For each case mean wind, tidal amplitude, and GW momentum flux profiles were determined for monthly and/or daily intervals (as appropriate). Also estimated in cases having diurnal variations in GW momentum fluxes were hourly profiles throughout a composite day.

[41] Our evaluation of relative radar performance revealed the following.

[42] 1. Measurement accuracies depend strongly on meteor counts and antenna beam patterns. Accuracies improve with higher meteor counts, smaller zenith angles, and more symmetric beam patterns enabled by crossed antennas.

[43] 2. SAAMER (on TdF), having ~12,000 meteors/day between 15 and 60° zenith angles (~120 meteors/hr in a 3-km altitude bin at ~90 km) performed best overall, yielding quite accurate mean wind, tidal amplitude, and GW momentum flux estimates for all test cases.

[44] 3. The BL meteor radar and DrAAMER (on KGI) performed comparably and very well, despite DrAAMER having ~30% smaller meteor counts (~8,000 meteors/day compared to ~12,000 total at BL, or ~80 and 120 meteors/hr in a 3-km altitude bin near the peak of the meteor distribution). However, DrAAMER yielded a consistently larger under-estimate of semidiurnal tide amplitudes (~5% rather than the ~2% seen at BL).

[45] 4. The SRO and YKF meteor radars having 6 kW peak power and antenna with only one polarization (having ~5,000 and 3,000 meteors/day, respectively, or 50 and 30 meteors/hr in 3 km) provided less accurate measurements and over more limited altitudes. They nevertheless described monthly mean winds and tidal amplitudes adequately, with the best results at central altitudes. Monthly mean and hourly composite-day GW momentum flux estimates were generally poor at lower and higher altitudes, but reasonable at ~85 to 90 km.

[46] More general conclusions obtained from intercomparisons of our various cases include the following.

[47] 5. Momentum flux estimates are more accurate when tidal amplitudes are small (or zero) and when GW amplitudes and momentum fluxes are large.

[48] 6. Momentum flux estimates are not significantly impacted by complexity of the GW field, including superposition, multiple scales and frequencies, and intermittency when meteor counts are sufficient.

[49] 7. Well configured radars (those having symmetric beam patterns (e.g., crossed Yagis) and/or more meteors at smaller zenith angles) capture daily and composite-day hourly variability of total winds and GW MFs well at altitudes where meteor counts are high.

[50] 8. Radars that have asymmetric beam patterns (single Yagi, linear polarization) and/or low meteor counts (less than ~25 meteors/hr in 3 km) will likely exhibit significant biases in estimates of daily mean winds and tidal amplitudes. They will likely also exhibit significant biases in estimates of hourly composite-day GW momentum fluxes and variability of these fields on longer time scales.

[51] Our assessment of meteor radar performance above assumed no radial velocity, range, or angle-of-arrival measurement uncertainties. Introducing such uncertainties would of course degrade measurement accuracies to some degree in all cases. Here we assess the likely impacts of radial velocity measurement uncertainties (assumed to include those accompanying range and angle-of-arrival uncertainties) for the magnitudes of the mean, tidal, and GW motions and momentum fluxes considered above.

[52] If we assume that RMS radial velocity uncertainties are ~1 to 2 ms^{-1} (which is reasonable for SAAMER), then these uncertainties are significantly less than typical radial velocity magnitudes arising from our specified mean winds and tidal and GW amplitudes, except at very small zenith angles for which uncertainties would imply very large (and errant) horizontal velocities. Fortunately, all five radars obtain very few valid radial velocity estimates at zenith angles <15°, with the large majority occurring between 20 and 60° in all cases (see Figure 1). As a result, radial velocity estimates typically include ~33 to 87% of the true horizontal velocities, which are statistically much larger than the assumed uncertainties. True vertical velocities also make relatively smaller contributions to radial velocities than the true horizontal velocities, because of the much smaller GW vertical velocities in general, and their relatively smaller contributions to measured radial velocities at the zenith angles at which most radial velocity estimates occur (~30 to 60° at BL, SCO, and YKF and at ~30 to 50° at TdF and KGI). Given this, we expect our observed zenith angle statistics to yield very accurate monthly mean and tidal wind estimates at all radars, with the major contributor to errors being small meteor counts.

[53] Accurate estimates of GW momentum fluxes require radial velocities at zenith angles having comparable contributions from true horizontal and vertical velocities. This implies smaller zenith angles because of the much larger horizontal than vertical velocities in a superposition of mean, tidal, and GW motions. As noted above, SAAMER and DrAAMER were specifically designed to optimize the potential for accurate measurements of large-scale (primarily horizontal) motions and GW momentum fluxes. For reference, most Doppler radars measurements of GW momentum fluxes have employed zenith angles of ~10 to 20° for these same reasons (see references cited above). Thus, including small zenith angles that enhance momentum flux measurement capabilities without adversely impacting large-scale horizontal wind measurements addresses both needs well. The zenith angle statistics seen in Figure 1 and the specific restriction in our analysis to zenith angles between 15 and 60° address both needs simultaneously.

[54] To assess qualitatively the impacts of radial velocity uncertainties on measurements of GW momentum fluxes, we assume that all meteors occur at the 35° zenith angle of maximum meteor counts for SAAMER and DrAAMER. We then evaluate the relative uncertainty of the momentum flux assessment using the "dual-beam" analysis of *Vincent and Reid* [1983] for a GW propagating zonally with superposed tidal winds and nominal radial velocity measurement uncertainties. The east and west radial velocities are given by

$$V_E = (u' + U_D + U_S)\sin\theta + w'\cos\theta + \Delta v_E' \quad (4)$$

and

$$V_W = -(u' + U_D + U_S)\sin\theta + w'\cos\theta + \Delta v_W' \quad (5)$$

where u' and w' are the horizontal and vertical GW velocities, U_D and U_S are the zonal diurnal and semidiurnal tidal motions (assuming negligible vertical tidal motions and no horizontal phase variations), $\theta = 35°$, $\Delta v_E'$ and $\Delta v_W'$ are additive radial velocity uncertainties selected from a distribution centered at zero with standard deviation chosen according to the expected radial velocity errors. Assuming all of the velocities in equations (4) and (5) are uncorrelated except for u' and w', which are in phase or antiphase, squaring, subtracting equation (5) from equation (4), and rearranging, the measured momentum flux may be written as

$$\begin{aligned}\langle u'w'\rangle_M &= \left(\langle V_E^2\rangle - \langle V_W^2\rangle - \langle \Delta v_E'^2\rangle + \langle \Delta v_W'^2\rangle\right)/2\sin(2\theta) \\ &= \langle u'w'\rangle_T - \left(\langle \Delta v_E'^2\rangle - \langle \Delta v_W'^2\rangle\right)/2\sin(2\theta) \quad (6)\end{aligned}$$

where angle brackets denote temporal averaging, the specified tidal terms in equations (4) and (5) cancel exactly, and $\langle u'w' \rangle_T$ is the true GW zonal momentum flux for the specified motion field. The fractional uncertainty in the measured momentum flux is then

$$\Delta\langle u'w' \rangle / \langle u'w' \rangle_T = -\left(\Delta v_E^2 - \Delta v_W^2\right) / \left[\langle u'w' \rangle_T 2\sin(2\theta)\right] \quad (7)$$

[55] Thus, fractional uncertainties are minimized if radial velocity uncertainty variance differences are small relative to the true GW momentum flux, as $2\sin(2\theta) = 1.88$ for the zenith angle specified. The largest magnitude of the numerator occurs if the radial velocity uncertainty variance is negligible in one beam. But for the uncertainties assumed above, this is $\langle \Delta v'^2 \rangle \sim 3$ m^2 s^{-2}, with likely values significantly smaller. By comparison, mean GW momentum fluxes in the MLT are typically $\sim$10 m^2 s^{-2}, with peak values $\sim$3 to 10 times larger, at most locations, with values over the Drake Passage "hotspot" expected (and measured, see *F10b*) to be $\sim$2 to 5 times larger. These values suggest a maximum fractional uncertainty of the momentum flux due to radial velocity uncertainties of $\sim$15% at typical sites and $\sim$5% in GW source hot spots.

[56] We anticipate range uncertainties comparable to the range resolution of 2 km and angle-of-arrival uncertainties of $\sim 1^\circ$ in zenith angle and $\sim 1.5^\circ$ in azimuth. These imply that altitude uncertainties are defined by zenith angle uncertainties near zenith angles of $\sim 60^\circ$ and by range uncertainties at smaller zenith angles. At all zenith angles, however, these values suggest altitude uncertainties comparable to or smaller than our chosen 3-km altitude bin. Thus range and angle-of-arrival uncertainties appear unlikely to significantly impact measurements of mean and tidal winds having large vertical scales or GW momentum fluxes that rely most on radial velocities occurring at smaller zenith angles. These results suggest that measurement uncertainties are likely to contribute much less to momentum flux uncertainties than inadequate definition of the mean, tidal, and GW fields due to low meteor counts arising due to low radar sensitivity or small averaging intervals and/or range bins.

[57] Several previous studies have assessed the potential for momentum flux measurement uncertainties due to inadequate sampling of the motion field. *Kudeki and Franke* [1998] and *Thorsen et al.* [2000] evaluated momentum flux measurements employing the "dual-beam" technique and concluded that very long averaging intervals were required to achieve statistical significance. *Kudeki and Franke* [1998] assumed the GW velocity fields to be defined by Gaussian distributions with a net momentum flux equal to 1% of that assuming a single GW was present and inferred a required integration time of 16 days. This assumption, however, is in contradiction to the strong correlations among component velocities that often occur when one or several large-amplitude GWs dominate the high-frequency motion field and the total momentum flux, as is often observed. In such cases, the averaging time implied by the *Kudeki and Franke* [1998] would decrease by 2 decades or more. Examples of dual-beam or multiple-beam measurements employing MF, VHF, and UHF radars that provide clear evidence for significant and variable GW momentum fluxes (magnitudes as large as $\sim$70 m^2 s^{-2}) occurring on time scales as short as a few hours or less include the following.

[58] 1. MLT measurements with the MF radar at Buckland Park, Australia revealed clear diurnal tide modulation of GW momentum fluxes with a modulation amplitude of $\sim$30 m^2 s^{-2} [*Fritts and Vincent*, 1987].

[59] 2. MLT measurements with the SOUSY VHF radar at Andoya, Norway revealed momentum fluxes (per unit density) of $\sim$66 m^2 s^{-2} over $\sim$3 h [*Reid et al.*, 1988].

[60] 3. Troposphere and stratosphere measurements using the MU VHF radar at Shigaraki, Japan for multibeam measurements of GW momentum fluxes over 6 days exhibited clear episodic enhancements as short as an hour simultaneously in multiple beams and spanning multiple altitudes [*Fritts et al.*, 1990].

[61] 4. MLT measurements employing the former VHF radar at Poker Flat, Alaska revealed clear anti-correlations between diurnal and semidiurnal tide winds and GW momentum fluxes over 4 and 16 day intervals exhibiting stronger momentum flux modulations ($\sim$5 to 10 m^2 s^{-2}) accompanying larger tidal amplitudes [*Wang and Fritts*, 1991].

[62] 5. MLT measurements spanning two 10-day intervals with the Jicamarca VHF radar in Peru exhibited daily mean momentum fluxes of $\sim$10 m^2 s^{-2} and maxima of $\sim$30 m^2 s^{-2}. Hourly profiles also exhibited significant coherence in altitude and time and maximum magnitudes of $\sim$60 m^2 s^{-2} [*Fritts et al.*, 1992].

[63] 6. MLT measurements with the MF radar at Buckland Park, Australia exhibited clear diurnal modulation of GW momentum fluxes by a large-amplitude 2-day wave [*Murphy and Vincent*, 1998].

[64] 7. MLT measurements employing the dual-beam Arecibo UHF radar revealed variable GW momentum fluxes often near zero, but with occasional maxima as large as $\sim$50 m^2 s^{-2} that were largely anti-correlated with the large-scale wind field [*Fritts et al.*, 2006b].

[65] 8. MLT measurements spanning $\sim$8 h employing the Arecibo UHF radar revealed very significant GW activity, but with momentum fluxes that were very small, suggesting ducting rather than vertical propagation [*Fritts and Janches*, 2008].

[66] A more recent study by *Vincent et al.* [2010] employed numerical simulations of test GW fields with a statistical model of radial velocity and angle-of-arrival uncertainties to evaluate the accuracy of meteor radar measurements of mean winds and GW velocity variances and momentum fluxes as functions of the meteor rate within a 2-km range bin. These authors concluded that mean winds could be determined with relatively few meteors, but that estimation of GW variances, and especially momentum fluxes, with small uncertainties required considerable averaging enabling large meteor counts. The meteor counts employed to assess measurement capabilities in the study ranged from 10 to 200 counts/hr.

[67] By comparison, our assessment above assumed a need for significant meteor counts, with the typical averaging interval for definition of mean and tidal winds and GW momentum fluxes being a month, but with mean wind and semidiurnal tide assessments also evaluated for one day or for one hour of a composite day for the month (hence 24 or 30 hr of data). Summarizing our discussion above, our assessments above imply a need for "adequate" meteor counts that differ depending on the quantity being measured.

Intervals of a day were seen to be reasonable for defining mean winds and diurnal tide amplitudes at KGI, TdF, and BL, with RMS uncertainties of ~2 ms^{-1} or less where meteor counts are high. However, daily estimates were much less accurate at SRO and YKF, and at the other three radars at the higher and lower altitudes, where overall meteor counts are low. Hourly estimates of total winds for a composite month were likewise reasonable for KGI, TdF, and BL, given the similar meteor counts required for daily assessments at these three sites, except where meteor counts were much smaller at the lowest and highest altitudes. Monthly momentum flux estimates were seen to be reasonable to very good at KGI, TdF, and BL, where meteor counts were high, but to suffer larger errors at the lowest and highest altitudes even at these sites, with greater errors typically accompanying more complex and variable tidal and GW motion fields. Hourly composite day estimates were also seen to reasonably capture the diurnal variability at KGI, TdF, and BL at intermediate altitudes, suggesting a potential ability, as noted by *F10b* at TdF, to examine correlations with tidal winds at these sites.

[68] Employing real meteor distributions observed during a test month for each of five radars (June of 2009, 2010, or 2011), these yielded meteor counts in a 3-km altitude bin at the peak of the meteor distribution for the month of ~80,000 at TdF, ~70,000 at BL, ~40,000 at KGI, and ~25,000 at SRO and YKF. Meteor counts at the upper and lower edges of these distributions varied by radar, but were typically smaller by ~2 to 4 times. Daily and composite-day hourly assessments employed ~3 and 4% of these meteor counts, respectively. Thus, in all cases, our meteor counts for each radar were significantly larger than those assessed by *Vincent et al.* [2010] near the peak of the meteor distribution.

[69] Assuming that accuracies vary as the signal-to-noise ratio (S/N) and thus as $N^{1/2}$, where N is the meteor count, we can compare our inferred accuracies with those of *Vincent et al.* [2010]. As noted above, the radars at BL, TdF, and KGI have peak monthly meteor counts of N ~40,000 to 80,000 in a 3-km altitude bin, with N ~10,000 to 25,000 at the edges of the distributions. These imply reductions by factors of ~15 to 25 in the mean wind measurement errors at the meteor distribution peak relative to the 5 ms^{-1} uncertainties displayed by *Vincent et al.* [2010] in Table 1, with reductions by factors of ~10 at the highest and lowest altitudes. Inspection of the monthly mean winds for the seven cases considered above suggests that our results are largely consistent with that expectation. Similarly, we expect error reductions of ~4 and 2 in the center and edge regions for daily mean winds, implying errors of ~1 to 3 ms^{-1}. These are largely consistent with the daily mean winds inferred for our Case 5 test fields displayed in Figure 8. Finally, meteor counts at SRO and YKF suggest monthly mean wind uncertainties smaller than the ~5 ms^{-1} uncertainties of *Vincent et al.* [2010] by ~12 and 5 in the center and edge regions. In these cases, our uncertainties seem to be comparable to, or somewhat larger than, those expected. We note, however, that the antenna patterns implied by the meteor locations shown in Figure 1 suggest significant asymmetries that likely also contribute to measurement errors.

[70] Applying the same factors to our momentum flux estimates, we expect to see errors of ~10 and 25% for the monthly means at the center and the edges of these distributions. Again, our results are consistent with these expectations, though with variations that depend on the complexity of our motions fields and the meteor distribution of each radar. Note, in particular, that *Vincent et al.* [2010] did not include tidal winds in their assessment, but that variable tidal winds can induce apparent mean winds and GW momentum fluxes if the meteor distribution is not approximately uniform in space and time. Our results also are relatively more accurate for cases having constant GW character throughout the month; they are less accurate for Cases 6 and 7 for which GWs are randomly distributed and likely more similar to the GW spectra specified by *Vincent et al.* [2010]. We cannot assess the contributions of the assumed radial velocity and angle-of-arrival uncertainties employed by *Vincent et al.* [2010] to the overall uncertainties displayed in their Table 1. However, our own assessment of radial velocity uncertainties above suggests that the majority of the measurement errors seen in our results can be attributed primarily to the expected dependence on meteor counts.

6. Conclusions

[71] Our assessment of meteor radar measurement capabilities presented in previous sections has demonstrated both (1) clear capabilities for quantitative measurements of mean winds, tides, and GW momentum fluxes by radars that achieve sufficiently high meteor counts and provide sensitivity to radial velocities at sufficiently small zenith angles, and (2) strong dependence of these measurement capabilities on radar power, beam geometry and sensitivity, and spatial and temporal meteor distributions.

[72] Meteor radars that combine high power, high meteor counts at small zenith angles, and symmetric beam patterns exhibit the smallest measurement errors. Those having low power, acquiring a majority of meteor detections at large zenith angles, and/or experiencing beam or meteor detection asymmetries exhibit much larger measurement uncertainties, thus either requiring longer averaging intervals or precluding the more challenging measurements, especially estimations of GW momentum fluxes.

[73] Monthly mean winds can typically be measured to within 1 ms^{-1} over ~15 to 20 km, with maximum accuracies between ~85 and 90 km, for radar frequencies near 35 MHz and having higher power that conventional meteor radars. These radars can also provide daily mean winds having accuracies of ~1 to 3 ms^{-1} where meteor counts are sufficient, even in the presence of large tidal motions. Monthly mean diurnal and semidiurnal tide amplitudes are also recovered very well by higher-power meteor radars yielding high meteor counts, but typically with amplitude under-estimates of a few %. Mean winds and tidal amplitudes are recovered very well employing meteors at zenith angles between 15 and 60° (the range employed in this study) because this range excludes (1) meteors at very small zenith angles for which amplitude or angle-of-arrival uncertainties could cause large and spurious horizontal velocity estimates and (2) meteors at very large zenith angles for which zenith angle uncertainties could cause significant errors in altitude estimates. The diurnal variation of meteor counts observed at each radar did not seem to adversely impact their estimates of mean and tidal wind fields, except possibly by allowing aliasing from other motions where meteor counts were very low.

[74] GW momentum flux estimates are challenging for meteor radars because of the large number of meteors required to adequately resolve differences in radial velocity variances at opposite azimuths. Nevertheless, accurate estimates over sufficiently long time scales (typically averages over 30 days) appear to be very feasible with sufficient meteor counts, even in the presence of significant tidal amplitudes and variability (i.e., with ∼60,000 or more meteors over a month in a 3-km altitude bin). Averages over many fewer hours, but sorted by hour within a monthly composite day also appear to yield reasonable estimates (see discussion of Figures 10, 12, and 14), though with less accuracy than monthly means. In these cases, only ∼2,500 meteors contribute in a 3-km bin, and the relatively reasonable accuracies at the peaks in the meteor distributions likely depend on the confident definition of effective horizontal motions over the composite day. This suggests (1) that diurnal variations in meteor counts do not impact hourly estimates for a composite day and (2) that daily or several day intervals may also yield reasonable estimates in cases where the large-scale motion field is not varying greatly, but further research is needed to define these conditions. Accuracies are also enhanced with high meteor counts at small zenith angles, given the greater sensitivity of these radial velocities to the correlations between horizontal and vertical velocities within the GW field. Importantly, meteor radars appear to measure momentum fluxes for stationary and propagating GWs, for complex GW superpositions, and for GW fields exhibiting significant intermittency equally well on monthly time scales.

[75] **Acknowledgments.** The research described here was performed under NSF grants ATM-0634650, ATM-0824742, and OPP-0839084. We are grateful for the valuable assistance of personnel at Estacion Astronomica Rio Grande (EARG) with the operations and maintenance of SAAMER. We are also grateful to the Secretaria for the Interministerial Commission of Sea Resources (SECIRM), the Brazilian Antarctic Program (PROANTAR), the National Institute for Science and Technology, Antarctic Environmental Research (INCT-APA), and the ATMANTAR/MCT/CNPq project, FAPERJ, for their support of this research and visits to Ferraz Station to install and service DrAAMER. Finally, the authors thank three anonymous reviewers for very valuable suggestions for revising the manuscript.

References

Acott, P. (2009), Mesospheric momentum flux studies over Fort Collins, CO, PhD dissertation, Colo. State Univ., Fort Collins.

Antonita, T. M., G. Ramkumar, K. K. Kumar, and V. Deepa (2008), Meteor wind radar observations of gravity wave momentum fluxes and their forcing toward the Mesospheric Semiannual Oscillation, *J. Geophys. Res.*, *113*, D10115, doi:10.1029/2007JD009089.

Brown, P. R. A. (1983), Aircraft measurements of mountain waves and their associated momentum flux over the British Isles, *Q. J. R. Meteorol. Soc.*, *109*, 849–865, doi:10.1002/qj.49710946211.

Clemesha, B. R., P. Batista, R. A. Buriti da Costa, and N. Schuch (2009), Seasonal variations in gravity wave activity at three locations in Brazil, *Ann. Geophys.*, *27*, 1059–1065, doi:10.5194/angeo-27-1059-2009.

Ern, M., P. Preusse, M. J. Alexander, and C. D. Warner (2004), Absolute values of gravity wave momentum flux derived from satellite data, *J. Geophys. Res.*, *109*, D20103, doi:10.1029/2004JD004752.

Espy, P. J., G. O. L. Jones, G. R. Swenson, and M. J. Taylor (2004), Tidal modulation of the gravity-wave momentum flux in the Antarctic mesosphere, *Geophys. Res. Lett.*, *31*, L11111, doi:10.1029/2004GL019624.

Espy, P. J., R. E. Hibbins, G. R. Swenson, J. Tang, M. J. Taylor, D. M. Riggin, and D. C. Fritts (2006), Regional variations of mesospheric gravity-wave momentum flux over Antarctica, *Ann. Geophys.*, *24*, 81–88, doi:10.5194/angeo-24-81-2006.

Fritts, D. C., and M. J. Alexander (2003), A review of gravity wave dynamics and effects in the middle atmosphere, *Rev. Geophys.*, *41*(1), 1003, doi:10.1029/2001RG000106.

Fritts, D. C., and D. Janches (2008), Dual-beam measurements of gravity wave momentum fluxes over Arecibo: Re-evaluation of wave structure, dynamics, and momentum fluxes, *J. Geophys. Res.*, *113*, D05112, doi:10.1029/2007JD008896.

Fritts, D. C., and T. Lund (2011), Gravity wave influences in the thermosphere and ionosphere: Observations and recent modeling, in *Aeronomy of the Earth's Atmosphere and Ionosphere*, edited by M. Abdu and D. Pancheva, pp. 109–130, Springer, New York.

Fritts, D. C., and R. A. Vincent (1987), Mesospheric momentum flux studies at Adelaide, Australia: Observations and a gravity wave/tidal interaction model, *J. Atmos. Sci.*, *44*, 605–619, doi:10.1175/1520-0469(1987)044<0605:MMFSAA>2.0.CO;2.

Fritts, D. C., and L. Yuan (1989), Measurement of momentum fluxes near the summer mesopause at Poker Flat, Alaska, *J. Atmos. Sci.*, *46*, 2569–2579, doi:10.1175/1520-0469(1989)046<2569:MOMFNT>2.0.CO;2.

Fritts, D. C., T. Tsuda, T. E. VanZandt, S. A. Smith, T. Sato, S. Fukao, and S. Kato (1990), Studies of velocity fluctuations in the lower atmosphere using the MU radar: II. Momentum fluxes and energy densities, *J. Atmos. Sci.*, *47*, 51–66, doi:10.1175/1520-0469(1990)047<0051:SOVFIT>2.0.CO;2.

Fritts, D. C., L. Yuan, M. H. Hitchman, L. Coy, E. Kudeki, and R. F. Woodman (1992), Dynamics of the equatorial mesosphere observed using the Jicamarca MST radar during June and August 1987, *J. Atmos. Sci.*, *49*, 2353–2371, doi:10.1175/1520-0469(1992)049<2353:DOTEMO>2.0.CO;2.

Fritts, D. C., S. A. Vadas, and Y. Yamada (2002), An estimate of strong local gravity wave body forcing based on OH airglow and meteor radar observations, *Geophys. Res. Lett.*, *29*(10), 1429, doi:10.1029/2001GL013753.

Fritts, D. C., S. L. Vadas, K. Wan, and J. A. Werne (2006a), Mean and variable forcing of the middle atmosphere by gravity waves, *J. Atmos. Sol. Terr. Phys.*, *68*, 247–265.

Fritts, D. C., D. Janches, D. M. Riggin, R. G. Stockwell, M. P. Sulzer, and S. Gonzalez (2006b), Gravity waves and momentum fluxes in the MLT using 430 MHz dual-beam measurements at Arecibo: 2. Frequency spectra, momentum fluxes, and variability, *J. Geophys. Res.*, *111*, D18108, doi:10.1029/2005JD006883.

Fritts, D. C., D. Janches, H. Iimura, W. K. Hocking, N. J. Mitchell, B. Fuller, B. Vandepeer, J. Hormaechea, C. Brunini, and H. Levato (2010a), Southern Argentina agile meteor radar (SAAMER): System design and initial measurements of large-scale winds and tides, *J. Geophys. Res.*, *115*, D18112, doi:10.1029/2010JD013850.

Fritts, D. C., D. Janches, and W. K. Hocking (2010b), Southern Argentina agile meteor radar (SAAMER): Initial assessment of gravity wave momentum fluxes, *J. Geophys. Res.*, *115*, D19123, doi:10.1029/2010JD013891.

Fritts, D. C., D. Janches, H. Iimura, W. K. Hocking, J. V. Bageston, and N. M. Pene (2012), Drake Antarctic Agile Meteor Radar first results: Configuration and comparison of mean and tidal wind and gravity wave momentum flux measurements with Southern Argentina Agile Meteor Radar, *J. Geophys. Res.*, *117*, D02105, doi:10.1029/2011JD016651.

Fukao, S., T. Sato, T. Tsuda, and S. Kato (1988), VHF Doppler radar determination of the momentum flux in the upper troposphere and lower stratosphere: Comparison between the three- and four-beam methods, *J. Atmos. Oceanic Technol.*, *5*(1), 57–69, doi:10.1175/1520-0426(1988)005<0057:VDRDOT>2.0.CO;2.

Hertzog, A., and F. Vial (2001), A study of the dynamics of the equatorial lower stratosphere by use of ultra-long-duration balloons, *J. Geophys. Res.*, *106*, 22,745–22,761, doi:10.1029/2000JD000242.

Hertzog, A., G. Boccara, R. A. Vincent, F. Vial, and P. Cocquerez (2008), Estimation of gravity wave momentum flux and phase speeds from quasi-Lagrangian stratospheric balloon flights. Part II: Results from the Vorcore campaign in Antarctica, *J. Atmos. Sci.*, *65*, 3056–3070, doi:10.1175/2008JAS2710.1.

Hines, C. O. (1960), 1960: Internal gravity waves at ionospheric heights, *Can. J. Phys.*, *38*(11), 1441–1481, doi:10.1139/p60-150.

Hitchman, M. H., K. W. Bywaters, D. C. Fritts, L. Coy, and E. Kudeki (1992), Mean winds and momentum fluxes over Jicamarca, Peru during June and August 1987, *J. Atmos. Sci.*, *49*, 2372–2383, doi:10.1175/1520-0469(1992)049<2372:MWAMFO>2.0.CO;2.

Hocke, K., and K. Schlegel (1996), A review of atmospheric gravity waves and traveling ionospheric disturbances: 1982–1995, *Ann. Geophys.*, *14*, 917–940.

Hocking, W. K. (2005), A new approach to momentum flux determinations using SKiYMET meteor radars, *Ann. Geophys.*, *23*, 2433–2439, doi:10.5194/angeo-23-2433-2005.

Hocking, W. K., and G. Kishore Kumar (2011), Long term behaviour of the MLT quasi 7 day wave at two radar-sites at northern polar latitudes, *J. Atmos. Sol. Terr. Phys.*, *73*, 1616–1628, doi:10.1016/j.jastp.2011.02.004.

Kim, Y.-J., S. D. Eckermann, and H.-Y. Chun (2003), A overview of the past, present and future of gravity-wave drag parameterization for numerical climate and weather prediction models, *Atmos. Ocean*, *41*, 65–98, doi:10.3137/ao.410105.

Kudeki, E., and S. J. Franke (1998), Statistics of momentum flux estimation, *J. Atmos. Sol. Terr. Phys.*, *60*, 1549–1553.

Kumar, K. K., T. M. Antonita, and S. T. Shelbi (2007), Initial results from SKiYMET meteor radar at Thumba (8.5°N, 77°E): 2. Gravity wave observations in the MLT region, *Radio Sci.*, *42*, RS6009, doi:10.1029/2006RS003553.

Lighthill, M. J. (1978), *Waves in Fluids*, Cambridge Univ. Press, Cambridge, U. K.

Lilly, D. K., and P. J. Kennedy (1973), Observations of a stationary mountain wave and its associated momentum flux and energy dissipation, *J. Atmos. Sci.*, *30*(6), 1135–1152, doi:10.1175/1520-0469(1973)030<1135:OOASMW>2.0.CO;2.

Lilly, D. K., J. M. Nicolls, P. J. Kennedy, J. B. Klemp, and R. M. Chervin (1982), Aircraft measurements of wave momentum fluxes over the Colorado Rocky Mountains, *Q. J. R. Meteorol. Soc.*, *108*, 625–642, doi:10.1002/qj.49710845709.

McIntyre, M. E. (1989), On dynamics and transport near the polar mesopause in summer, *J. Geophys. Res.*, *94*, 14,617–14,628, doi:10.1029/JD094iD12p14617.

Meyer, W., R. Siebenmorgen, and H.-U. Widdel (1989), Estimates of gravity wave momentum fluxes in the winter and summer high mesosphere over Scandinavia, *J. Atmos. Terr. Phys.*, *51*(4), 311–319.

Mitchell, N. J., and C. L. Beldon (2009), Gravity waves in the mesopause region observed by meteor radar: 1. A simple measurement technique, *J. Atmos. Sol. Terr. Phys.*, *71*, 866–874, doi:10.1016/j.jastp.2009.03.011.

Murayama, Y., T. Tsuda, and S. Fukao (1994), Seasonal variation of gravity wave activity in the lower atmosphere observed with the MU radar, *J. Geophys. Res.*, *99*(D11), 23,057–23,069, doi:10.1029/94JD01717.

Murphy, D. J., and R. A. Vincent (1993), Estimates of momentum flux in the mesosphere and lower thermosphere over Adelaide, Australia, from March 1985 to February 1986, *J. Geophys. Res.*, *98*(D10), 18,617–18,638, doi:10.1029/93JD01861.

Murphy, D. J., and R. A. Vincent (1998), Mesospheric momentum fluxes over Adelaide during the 2-day wave: Results and interpretation, *J. Geophys. Res.*, *103*(D22), 28,627–28,636, doi:10.1029/1998JD200001.

Nakamura, T., T. Tsuda, M. Yamamoto, S. Fukao, and S. Kato (1993), Characteristics of gravity waves in the mesosphere observed with the middle and upper atmosphere radar: 1. Momentum flux, *J. Geophys. Res.*, *98*(D5), 8899–8910, doi:10.1029/92JD02978.

Nappo, C. J. (2002), *An Introduction to Atmospheric Gravity Waves*, Academic, San Diego, Calif.

Nastrom, G. D., and D. C. Fritts (1992), Sources of mesoscale variability of gravity waves, I: Topographic excitation, *J. Atmos. Sci.*, *49*, 101–110, doi:10.1175/1520-0469(1992)049<0101:SOMVOG>2.0.CO;2.

Placke, M., P. Hoffmann, E. Becker, C. Jacobi, W. Singer, and M. Rapp (2011), Gravity wave momentum fluxes in the MLT—Part II: Meteor radar investigations at high and midlatitudes in comparison with modeling studies, *J. Atmos. Sol. Terr. Phys.*, *73*, 911–920.

Reid, I. M., and R. A. Vincent (1987), Measurements of mesospheric gravity wave momentum fluxes and mean flow accelerations at Adelaide, Australia, *J. Atmos. Terr. Phys.*, *49*, 443–460, doi:10.1016/0021-9169(87)90039-0.

Reid, I. M., R. Rüster, P. Czechowsky, and G. Schmidt (1988), VHF radar measurements of momentum flux in the summer polar mesosphere over Andenes (69ºN, 16ºE), Norway, *Geophys. Res. Lett.*, *15*, 1263–1266, doi:10.1029/GL015i011p01263.

Sato, K. (1990), Vertical wind disturbances in the troposphere and lower stratosphere observed by the MU radar, *J. Atmos. Sci.*, *47*(23), 2803–2817, doi:10.1175/1520-0469(1990)047<2803:VWDITT>2.0.CO;2.

Sato, K. (1993), Small-scale wind disturbances observed by the MU radar during the passage of Typhoon Kelly, *J. Atmos. Sci.*, *50*(4), 518–537, doi:10.1175/1520-0469(1993)050<0518:SSWDOB>2.0.CO;2.

Sato, K. (1994), A statistical study of the structure, saturation and sources of inertio-gravity waves in the lower stratosphere observed with the MU radar, *J. Atmos. Terr. Phys.*, *56*(6), 755–774, doi:10.1016/0021-9169(94)90131-7.

Smith, R. B., B. K. Woods, J. Jensen, W. A. Cooper, J. D. Doyle, Q. Jiang, and V. Grubisic (2008), Mountain waves entering the stratosphere, *J. Atmos. Sci.*, *65*, 2543–2562, doi:10.1175/2007JAS2598.1.

Swenson, G. R., R. Haque, W. Yang, and C. S. Gardner (1999), Momentum and energy fluxes of monochromatic gravity waves observed by an OH imager at Starfire Optical Range, New Mexico, *J. Geophys. Res.*, *104*(D6), 6067–6080, doi:10.1029/1998JD200080.

Thorsen, D., S. J. Franke, and E. Kudeki (2000), Statistics of momentum flux estimation using the dual coplanar beam technique, *Geophys. Res. Lett.*, *27*, 3193–3196, doi:10.1029/1999GL011196.

Tsuda, T., Y. Murayama, M. Yamamoto, S. Kato, and S. Fukao (1990), Seasonal variation of momentum flux in the mesosphere observed with the MU radar, *Geophys. Res. Lett.*, *17*, 725–728, doi:10.1029/GL017i006p00725.

Vincent, R. A., and I. M. Reid (1983), HF Doppler measurements of mesospheric momentum fluxes, *J. Atmos. Sci.*, *40*, 1321–1333, doi:10.1175/1520-0469(1983)040<1321:HDMOMG>2.0.CO;2.

Vincent, R. A., S. Kovalam, I. M. Reid, and J. P. Younger (2010), Gravity wave flux retrievals using meteor radars, *Geophys. Res. Lett.*, *37*, L14802, doi:10.1029/2010GL044086.

Wang, D.-Y., and D. C. Fritts (1990), Mesospheric momentum fluxes observed by the MST radar at Poker Flat, Alaska, *J. Atmos. Sci.*, *47*, 1512–1521, doi:10.1175/1520-0469(1990)047<1512:MMFOBT>2.0.CO;2.

Wang, D.-Y., and D. C. Fritts (1991), Evidence of gravity wave-tidal interaction observed near the summer mesopause at Poker Flat, Alaska, *J. Atmos. Sci.*, *48*, 572–583, doi:10.1175/1520-0469(1991)048<0572:EOGWIO>2.0.CO;2.

Zhang, X., J. M. Forbes, and M. E. Hagan (2010a), Longitudinal variation of tides in the MLT region: 1. Tides driven by tropospheric net radiative heating, *J. Geophys. Res.*, *115*, A06316, doi:10.1029/2009JA014897.

Zhang, X., J. M. Forbes, and M. E. Hagan (2010b), Longitudinal variation of tides in the MLT region: 2. Relative effects of solar radiative and latent heating, *J. Geophys. Res.*, *115*, A06317, doi:10.1029/2009JA014898.